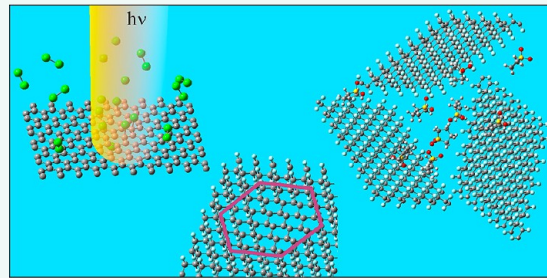


Halogenated Graphenes: Rapidly Growing Family of Graphene Derivatives

František Karlický, Kasibhatta Kumara Ramanatha Datta, Michal Otyepka,* and Radek Zbořil*

Regional Centre of Advanced Technologies and Materials, Department of Physical Chemistry, Faculty of Science, Palacký University, 17. listopadu 1192/12, 771 46 Olomouc, Czech Republic

ABSTRACT Graphene derivatives containing covalently bound halogens (graphene halides) represent promising two-dimensional systems having interesting physical and chemical properties. The attachment of halogen atoms to sp^2 carbons changes the hybridization state to sp^3 , which has a principal impact on electronic properties and local structure of the material. The fully fluorinated graphene derivative, fluorographene (graphene fluoride, C_1F_1), is the thinnest insulator and the only stable stoichiometric graphene halide (C_1X_1). In this review, we discuss structural properties, syntheses, chemistry, stabilities, and electronic properties of fluorographene and other partially fluorinated, chlorinated, and brominated graphenes. Remarkable optical, mechanical, vibrational, thermodynamic, and conductivity properties of graphene halides are also explored as well as the properties of rare structures including multilayered fluorinated graphenes, iodine-doped graphene, and mixed graphene halides. Finally, patterned halogenation is presented as an interesting approach for generating materials with applications in the field of graphene-based electronic devices.



KEYWORDS: graphene · graphene semiconductor · fluorination · doping · magnetic graphene · band gap opening · chlorographene · chlorination · graphene oxide · graphene dot

Graphene, comprising a single layer of sp^2 -bonded carbon atoms arranged in a honeycomb lattice, was the first two-dimensional atomic crystal to be identified. Since its initial isolation in 2004, many studies have shown that this one-atom-thick material of carbon uniquely combines superior mechanical strength, remarkably high electronic and thermal conductivities, high surface area, and impermeability to gases, in addition to many other desirable properties, all of which make it highly attractive for numerous applications.¹ Many of the unique physical properties of graphene stem from its unusual electronic structure near the Fermi level.² The ability to tailor its properties, especially the opening of a band gap, is critical for its potential use in several (opto)electronic applications.³

In the past few years, covalently modified graphene derivatives prepared by attachment of hydrogen, halogens, or other atoms have attracted considerable interest for their potential applications (e.g., in electronic devices).^{4–6} The relative simplicity of

atomic adsorbates allows them to be also well described by theoretical calculations.⁷ The idea to fully hydrogenate graphene was put forward in 2003 ahead of graphene's isolation, and several possible geometrical structures were considered,⁸ even though at that stage it was clearly a hypothetic material. In 2007, fully hydrogenated graphene was named graphane by Sofo *et al.*,⁹ who also discussed its electronic properties and its fluorinated counterpart. Two years later, graphane was synthesized as a stable material under ambient conditions by exposure of graphene to cold hydrogen plasma.^{10,11}

The fully fluorinated graphene counterpart, fluorographene (graphene fluoride, C_1F_1), was prepared experimentally in 2010 (refs 12–14) by chemical and mechanical exfoliation of graphite fluoride, that is, by approaches that had been successfully applied to prepare graphene from graphite. Graphite fluoride is a well-known graphite derivative (fluorine-intercalated compound)¹⁵ with covalent C–F bonds. Although bulk graphite fluoride has been used as a lubricant

* Address correspondence to
michal.otyepka@upol.cz,
radek.zboril@upol.cz.

Received for review May 13, 2013
and accepted June 28, 2013.

Published online June 28, 2013
10.1021/nn4024027

© 2013 American Chemical Society

for nearly 100 years and has also been exploited as an excellent electrode material in primary lithium batteries, graphene fluoride was not experimentally realized until 2010. Alternative ways of preparing fluorinated graphene^{12,16} or graphite^{17,18} by cold plasma were developed simultaneously. However, this approach often generates nonstoichiometric fluorinated graphenes (C_1F_a , $a < 1$). The attachment of fluorine atoms to sp^2 carbons changes the hybridization state to sp^3 (Figure 1a and Figure 1b), which significantly affects the electronic properties and local structure of the material but preserves the 2D hexagonal symmetry. Such structural changes induce opening of the zero band gap of graphene at the K point and lead to loss of the π -conjugated electron cloud above and below the graphene plane. The charge carrier mobility has been shown to be 3 orders of magnitude smaller for fluorographene in comparison to graphene, and fluorographene behaves like an insulator with a minimal direct band gap at the Γ point (Figure 1c,d).

To date, dozens of experimental and theoretical papers on halogenated graphenes have been published. Besides the stoichiometric fluorographene, numerous partially fluorinated graphenes have also been synthesized,^{19–24} where the degree of fluorination enables control over the electronic properties, which might be utilized in band gap engineering of 2D carbon-based materials. Contrary to fluorographene, the fully chlorinated counterpart has not been yet prepared, while partially chlorinated^{25–28} or brominated^{27,28} graphene derivatives have been reported very recently. Halogenated graphenes exhibit a plethora of remarkable and interesting electronic, optical, thermal, electrocatalytic, magnetic, mechanical, biological, and chemical properties in comparison with their graphene counterparts.

Here, we classify the graphene halides and review preparation approaches, properties, and applications of halogenated graphenes. The review provides a complex overview as it considers both experimental and theoretical aspects of graphene halogenation. First, the synthesis of graphene halides is discussed. Next, properties of fluorographene and partially fluorinated graphenes are summarized including insightful theoretical studies. These sections focus on structural and vibrational properties, which can be used as fingerprints of the considered materials, as well as electronic, optical, and mechanical properties of graphene halides, which are important from an application perspective. Next, we summarize recent progress on chlorinated and brominated graphenes from both theoretical and experimental standpoints. Finally, we discuss patterned structures on graphene.

Synthesis of Graphene Halides. Synthesis of Fluorographene and Fluorinated Graphenes. There are two main methods to prepare fluorographenes.^{12,13,16} One approach involves transformation of graphenes to fluorographenes by fluorination using an appropriate fluorinating agent (see below).^{12,16} The other procedure utilizes chemical or mechanical exfoliation

VOCABULARY:: **graphene derivatives** – a class of materials having two-dimensional scaffold, which are derived from graphene by covalent attachment of atoms, functional groups or molecular moieties. Graphane, graphene oxide, and fluorographene represent the typical examples of graphene derivatives; **fluorographene** – stoichiometric C_1F_1 derivative of graphene with the fluorine atom attached to each carbon atom thus having sp^3 hybridization. Fluorographene can be prepared by graphene fluorination or exfoliation of graphite fluoride. Fluorographene represents still the only stoichiometric graphene halide stable at ambient conditions; **halogenated graphenes** – graphene derivatives, in which some carbon atoms are covalently linked with halogen atoms. The carbon atoms linked with halogens have sp^3 hybridization and others have sp^2 hybridization. The physicochemical properties of graphene halides are strongly dependent on a degree of halogenation; **patterned halogenation** – the outcome of placing masks or metal grids over graphene during halogenation process is known as patterned halogenation. Uncovered regions of the graphene become halogenated and the masked regions remain intact and can be used as conductive pathways for device fabrication or construction of graphene superstructures; **band gap engineering** – graphene lacks a band gap because its valence and conduction bands touch each other, and it is labeled as a semimetal. The lacking band gap limits usage of graphene in contemporary electronic devices. The band structure of graphene can be modified to open the band gap by many strategies, e.g., halogenation, oxidation, hydrogenation or noncovalent attachment of various molecules and species. A complex way how to open and tune the band gap in graphene and its derivatives is termed as band gap engineering;

of pristine graphite fluoride, i.e., the same techniques that have been successfully applied for the preparation of graphene from graphite.^{29,30}

Fluorographene can be prepared by fluorinating graphene using XeF_2 at various temperatures under an inert atmosphere (Figure 2a)^{12,31} or at room temperature (30 °C).¹⁶ The room temperature preparation of fluorographene involves fluorinating graphene supported on a silicon-on-insulator substrate using XeF_2 gas, which selectively etches the Si underlayer and fluorinates both sides of the graphene to form fully fluorinated graphene with a dominant stoichiometry of $C_{1.0}F_{1.0}$.¹⁶ In addition, fluorination of highly oriented pyrolytic graphite (HOPG) by fluorine gas under high temperature (600 °C) and subsequent chemical exfoliation has been shown to yield a nonstoichiometric fluorographene ($C_1F_{0.7}$) of low quality owing to numerous structural defects caused by the harsh preparation conditions.¹⁷ It should be noted, that fluorination of graphene grown by chemical vapor deposition (CVD) on copper has been reported to yield a single side partially fluorinated graphene with dominant stoichiometry of $CF_{0.25}$.¹⁶

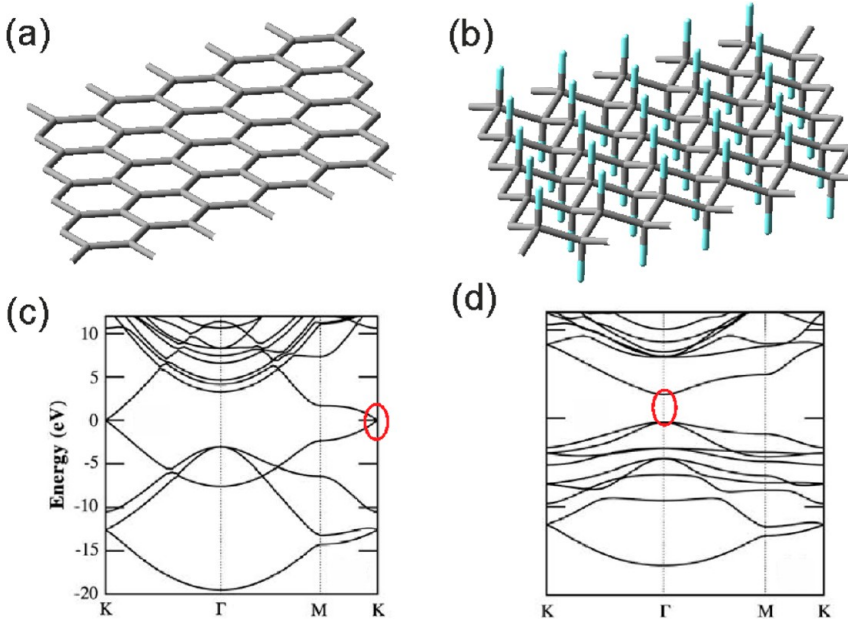


Figure 1. (a) Hexagonal structure of sp^2 carbons in graphene. (b) Transformation to sp^3 carbons by fluorination in the chair conformation of fluorographene. Electronic band structures of (c) graphene and (d) fluorographene. The original graphene zero band gap at the K point is opened to a band gap with minimal value of several eV at the Γ point (red circles).

Stoichiometric fluorographene can also be prepared by a top-down approach employing mechanical^{12,14} or chemical^{13,23,32} exfoliation of graphite fluoride. Graphene fluoride in the form of colloidal suspensions can be obtained by chemically etching bulk graphite fluoride *via* sonication in the presence of sulfolane,¹³ dimethylformamide (DMF),³² or N-methyl-2-pyrrolidone (NMP)²³ (Figure 2b). In this process, the solvent molecules intercalate within the interlayers, weakening the van der Waal's interactions between neighboring layers and facilitating the exfoliation of graphite fluoride into colloidal fluorographenes. In the case of mechanical exfoliation, the as prepared fluorographene monolayers are of high quality and are suitable for physical experiments. However, such an approach is difficult to scale-up for potential applications. On the other hand, chemical exfoliation enables preparation of large amounts of graphene fluoride. However, polydisperse systems are formed containing one- and few-layer fluorographenes. Nonetheless, the solution processability of fluorographene colloids could be advantageous in the field of coatings, polymer nanocomposites, etc.

Fluorinated graphene with different fluorine loadings can be achieved by fluorinating graphene or chemically etching nonstoichiometric graphene fluoride. Briefly, fluorination of graphene or reduced graphene oxide sheets (mono- and multilayered) is usually carried out in plasmas containing CF_4 (refs 33, 34) and SF_6 ,³⁵ XeF_2 ,^{36,37} fluoropolymers²⁰ or Ar/F_2 (ref 38) as fluorinating agents. The fluorine content of the resulting fluorinated graphenes can be varied by changing the plasma treatment time as well as the fluorinating agent.^{33,36,39}

Recently, Ruoff and co-workers²⁰ have developed a versatile and environmentally friendly approach for selective or patterned fluorination of graphene (on a SiO_2/Si substrate) using the fluoropolymer CYTOP combined with laser irradiation. In this method, direct contact between CYTOP and the graphene surface is achieved by transferring graphene films on Cu foil onto a SiO_2/Si substrate coated with CYTOP. After laser irradiation, photon-induced decomposition of CYTOP generates many active intermediates, such as CF_x and F radicals, which react with sp^2 hybridized graphene forming C–F sp^3 bonds (Figure 2c). This process yields single side fluorination (25% coverage) as the active fluorine species cannot penetrate through the SiO_2/Si substrate.

Similar to the isolation of fluorographenes from bulk graphite fluoride *via* chemical etching, fluorinated graphenes can be exfoliated from graphite fluoride with different fluorine contents in various solvents with/without surfactants *via* sonication^{19,24,40} or mechanical exfoliation.⁴¹ Fluorinated graphenes with compositions $CF_{0.25}$ and $CF_{0.5}$ have been obtained by exfoliating graphite fluoride with fluorinated ionic liquids, as described by Zheng *et al.*¹⁹ Very recently, multilayer semi-ionically fluorinated graphene was prepared using a one-pot synthesis employing liquid ClF_3 and graphite (5 h). The obtained sample was subsequently mechanically exfoliated to single and bilayer films.^{42,43}

Fluorine-doped multilayered graphene (10 wt %, *i.e.*, 6.6 atom %) has been synthesized using an arc discharge process in which a hollow graphite rod is filled with powdery graphite fluoride.²² The fluorine content of the graphene matrix can also be tuned

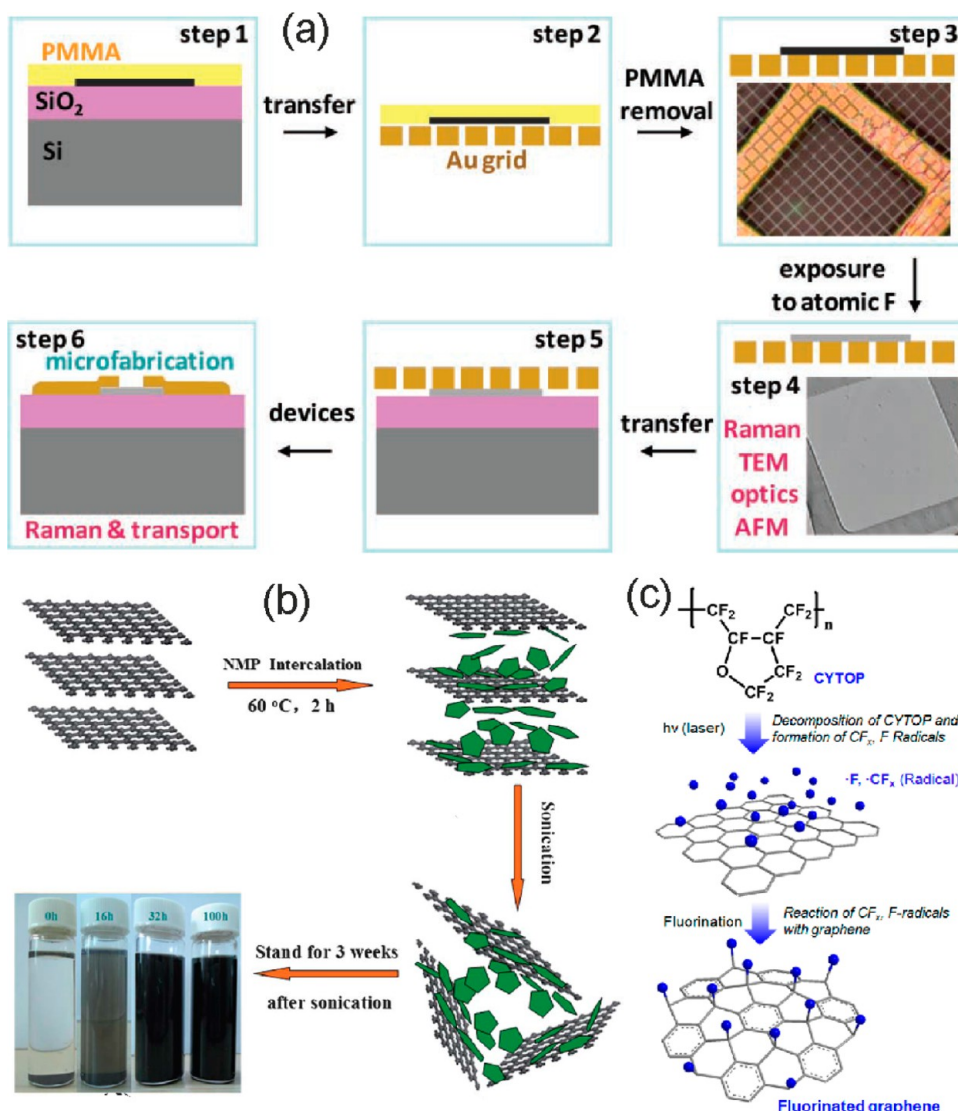


Figure 2. (a) Various steps involved in the fluorination of graphene (PMMA – poly(methyl methacrylate)). Reprinted with permission from ref 12. Copyright 2010 Wiley. (b) Schematic of the NMP intercalation and exfoliation fabrication processes used to prepare CF dispersions. Reprinted with permission from ref 23. Copyright 2012 Royal Society of Chemistry. (c) Scheme showing the mechanism of fluorination using CYTOP and laser irradiation. Reprinted from ref 20. Copyright 2012 American Chemical Society.

by the chemical reaction of graphene oxide with hydrofluoric acid.²¹ Fluorination of graphene oxide can be done by exposing graphene oxide to anhydrous HF vapors at various temperatures⁴⁴ or photochemically at room temperature using HF solution.⁴⁵

Synthesis of Other Halogenated Graphenes. Recently, a nondestructive and patternable photochemical chlorination treatment of single- and few-layer graphene has been used to produce a material with stoichiometry $CCl_{0.08}$.²⁵ The chemical patterning was achieved using a chlorine-resistant Al/Ti mask to protect selected regions of graphene from photochlorination. In this approach, chlorine radicals covalently attach to the basal carbon atoms of the graphene (C–Cl), transforming from a sp^2 to sp^3 configuration and creating high structural disorder. The chlorine plasma technique allows controlled p-type doping

of graphene sheets and graphene nanoribbons.²⁶ The chlorination of graphene occurs in two stages: in the first stage, chlorination occurs rather nondestructively and reversibly, whereas in the second stage at longer exposure times (>2 min), larger-area defects begin to form irreversibly. Graphene nanoribbons (GNR) supported on SiO₂/Si and exposed to Cl plasma (1 min) showed a 1.3–2.2 fold increase in conductance (in ambient air). Similarly, after Cl plasma treatment for 10 s, graphene sheets showed a slight increase (with respect to GNR) in conductance, whereas longer exposure resulted in reduced conductivity. Compared to fluorination and hydrogenation, the chlorine plasma reaction with graphene exhibits the slowest kinetics, showing only a slow increase in disorder with reaction time.

Recently, Rao and co-workers²⁸ prepared few-layer chlorinated and brominated graphenes up to 30 atom %

($\text{CCl}_{0.43}$) and 5 atom % ($\text{CBr}_{0.05}$), respectively, using ultraviolet (UV) irradiation in liquid chlorine or liquid bromine media. A microwave-spark (MiW-S) assisted reaction has also been developed that allows the direct production of Cl and Br-functionalized monolayer graphene sheets from graphite.²⁷ During microwave irradiation, graphite was shown to expand to 200 times its original volume accompanied by luminous sparks and moderate ionization of the halogens (X^+). The ionized halogen atoms readily attacked the π -ring of graphene, resulting in halogenation, probably *via* an electrophilic substitution mechanism. The amount of Cl atoms on the graphene sheets was up to 21 atom % ($\text{CCl}_{0.27}$), whereas Br was 4 atom % ($\text{CBr}_{0.04}$), as measured by XPS analysis.²⁷ Chlorination was shown to be more effective than bromination as liquid Cl_2 is more reactive than Br_2 .^{27,28} Thermal annealing or laser irradiation of the prepared chlorinated graphene samples completely removed the chlorine to obtain pristine graphene.^{27,28} Interestingly, the halogen atoms in the resulting CX could be substituted/modified by other organic functional groups under conventional organic reaction conditions, which opens up other possibilities for preparing graphene derivatives.²⁷

Iodine-doped graphenes with an iodine loading of 3 atom % have been prepared by direct heating of camphor and I_2 .⁴⁶ In addition, exfoliation of graphene oxide and I_2 under ultrasonic treatment followed by thermal annealing at various temperatures (500–1100 °C) has been shown to generate iodine-doped graphenes (1.2–0.8 wt %, *i.e.*, ~0.1 atom %).⁴⁷ Very recently, halogenated graphenes have been prepared by the thermal exfoliation of graphite oxide under different gaseous halogen atmospheres (chlorine, bromine, or iodine),⁴⁸ generating halogenated graphenes with doping levels of 5.9, 9.93, and 2.3 wt % (2.1, 1.6, and 0.2 atom %) for Cl, Br, and I, respectively.

Fluorographene (Graphene Fluoride, $\text{C}_{1.0}\text{F}_{1.0}$). *Structural Properties of CF.* The structure of graphene can be derived from the structure of the 3D pristine material bulk graphite, which comprises stacks of graphene layers that are weakly coupled by van der Waals forces. Similarly, the geometrical structure of fully fluorinated graphene (fluorographene, graphene fluoride, CF) can be deduced from the structure of bulk graphite mono-fluoride (CF_n). Graphite fluoride has been shown to consist of weakly bound stacked fluorographene layers, and its most stable conformation (predicted for the monocrystal) contains an infinite array of trans-linked cyclohexane chairs with covalent C–F bonds in an AB stacking sequence^{49,50} (Figure 3a), in agreement with the model proposed from X-ray powder diffraction experiments by Touhara *et al.* (Figure 3b, AA' stacking).⁵¹ However, for many years, it was also believed to contain stacked structures with cis–trans-linked cyclohexane boats, as predicted from NMR second moment measurements (Figure 3c,d).⁵² Various stacking sequences of (CF_n ,

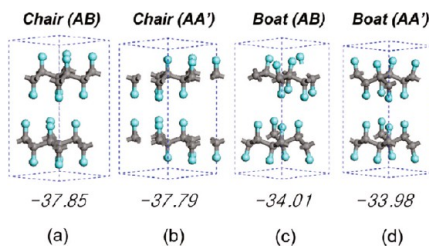


Figure 3. Structural models of graphite fluoride optimized by GGA DFT calculations (gray and cyan colors indicate carbon and fluorine atoms, respectively). The numbers underneath each structure show the calculated heats of formation (in kcal/mol). Reprinted from ref 49. Copyright 2010 American Chemical Society.

are very close on the energy scale, suggesting that in the structure of (CF_n), prepared, for example, by fluorination, a statistical distribution of various sequences can occur.

To gain a better understanding of the structural properties of fluorographene, prototype stoichiometric configurations for fluorographene, for example, chair, boat, zigzag (stirrup), and armchair (Figure 4), have been studied theoretically. On the basis of first-principles density functional theory (DFT) calculations, the chair conformation was predicted to be most stable,^{53,54} analogous to fully hydrogenated graphene (graphane). The zigzag (stirrup) configuration was found to be more stable than the boat and armchair configurations, and its formation energy was predicted to be only slightly higher than that of the chair configuration. The energy differences between the various configurations were more pronounced for fluorographene than for fully hydrogenated graphene, but they were of the same order of magnitude. The results suggested that the experimentally observed fluorographene is unlikely to be in a single crystal form of chair, boat, or stirrup because each of those structures has only one or two distinctive in-plane lattice spacings, in contrast to the wide range of distributions observed experimentally. Wide distributions of lattice parameters for both fluorographene⁵⁴ and graphane⁵⁵ have been predicted by simulations with large supercells containing randomly distributed adsorbates, suggesting other locally stable configurations (*e.g.*, twist-boat-chair or epoxy-pair conformations) are possible.

Nonetheless, in calculations of electronic, optical, and other properties of fluorographene (see below), the chair conformation is usually considered the most stable (Figure 4), taking advantage of the high symmetry. It corresponds to a unit cell of two fluorine and two carbon atoms ($P-3M1$ (164) space group or D_{3d} point group) with translation vectors $a_1 = d(\sqrt{3}/2, 1/2, 0)$, and $a_2 = d(\sqrt{3}/2, -1/2, 0)$, and lattice parameter predicted from standard generalized gradient approximation (GGA) DFT calculations of $d = 2.61 \text{ \AA}$; the corresponding C–C and C–F bond lengths are 1.58 Å and 1.38 Å, respectively.^{53,56–59} The fluorographene lattice structure and the real and reciprocal space elements

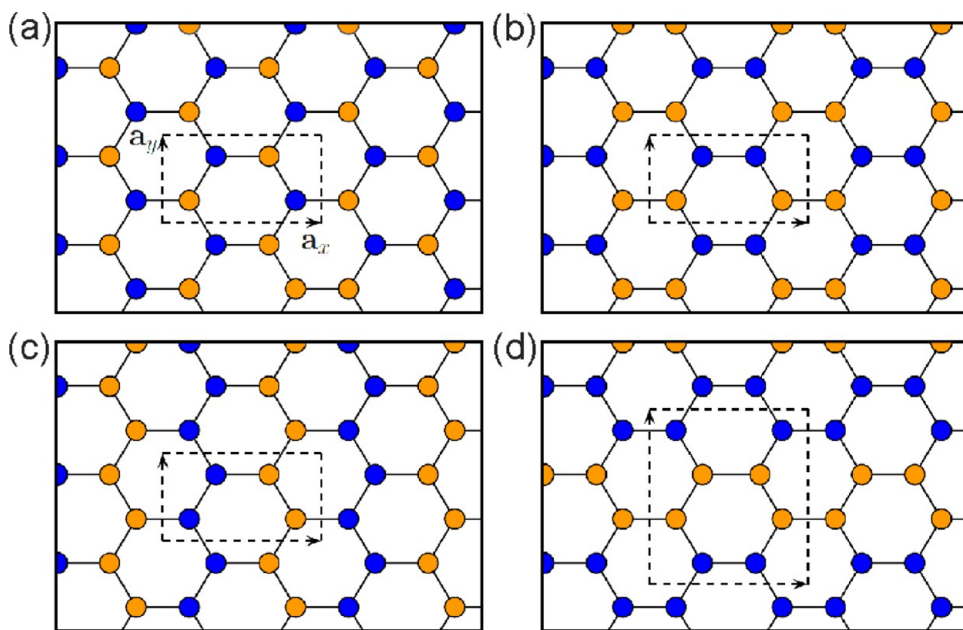


Figure 4. Four different configurations of fluorographene: (a) chair, (b) boat, (c) zigzag (stirrup), and (d) armchair configurations. The different colors (shades) represent fluorine atoms above and below the graphene plane. The supercell used to calculate the elastic constants is indicated by the dashed box (see sections below). Reprinted with permission from ref 53. Copyright 2010 American Physical Society.

are shown Figure 5. The calculated structural parameters are not very sensitive to density functional choice (e.g., the C–C and C–F bond lengths are predicted to be 1.57 Å and 1.36 Å, respectively, using the hybrid HSE06 functional).⁵⁸ However, DFT calculations are generally sensitive to the choice of exchange-correlation functional, and therefore it is highly desirable to cross-check the calculated data.

Electron diffraction analysis of fluorographene has confirmed the existence of a hexagonal crystalline structure^{12,13,17} and stoichiometry¹³ equivalent to that of graphite fluoride (Figure 6). It has been shown that the retention of hexagonal crystalline order for fluorographene is similar to that of graphene with 1% expansion of the unit cell (Figure 7):^{12,17} compare the C₁F₁ experimental lattice constant of 2.48 Å versus 2.46 Å for graphene. The increased unit cell and in-plane lattice constant of CF is expected as the carbon atoms making C–C bonds are converted from a sp² to sp³ configuration during the fluorination process accompanied by an increase in the C–C bond length. The bonding and composition of fluorographenes has also been characterized by X-ray photoelectron spectroscopy (XPS) and Raman spectroscopy. XPS analysis showed the majority of bonding in this material is C–F (86%), with smaller fractions of C–F₂ and C–F₃ species (owing to defects at the free edges).¹⁶ These defects are believed to originate during the graphene transfer process and vary from one support to another; for example, larger quantities of C–F_n ($n > 1$) species were observed for fluorinated graphene samples on a silicon-on-insulator substrate compared to those on

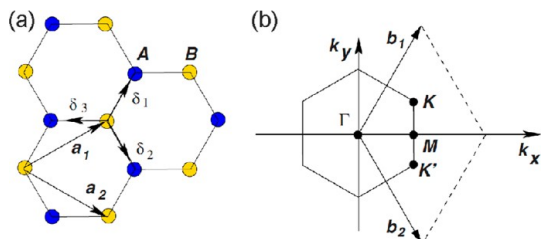


Figure 5. (a) Honeycomb lattice structure of fluorographene, made out of two interpenetrating triangular lattices (a_1 and a_2 are the lattice unit vectors, and δ_i , $i = 1, 2, 3$ are the nearest-neighbor vectors) (b) corresponding to the Brillouin zone, the reciprocal basis vectors and high-symmetry points Γ , M , and K . Reprinted with permission from ref 2. Copyright 2009 American Physical Society.

copper.¹⁶ Notably, the support also seems to affect the fluorine content. Early experiments suggested that the lateral dimensions of fluorographene sheets typically range from 200 nm to 2 μ m (see Figure 6).^{12,13}

Definitive proof of the presence of fluorographene monolayers has been obtained by atomic force microscopy (AFM) experiment (Figure 8), which revealed that the monolayer is 0.67–0.87 nm thick, although multi-layered sheets ca. 2–4 nm thick were also detected.^{13,17} The experimental values (allowing for the effects of signal noise and the presence of solvent impurities on the surface or support), were in agreement with theoretical estimates of the thickness of a single CF layer of 0.62 nm and were certainly less than the predicted thickness of a two-layer graphene fluoride system of 1.24 nm.¹³

Electronic Properties of CF. The I–V characteristics of fully fluorinated graphene are strongly nonlinear

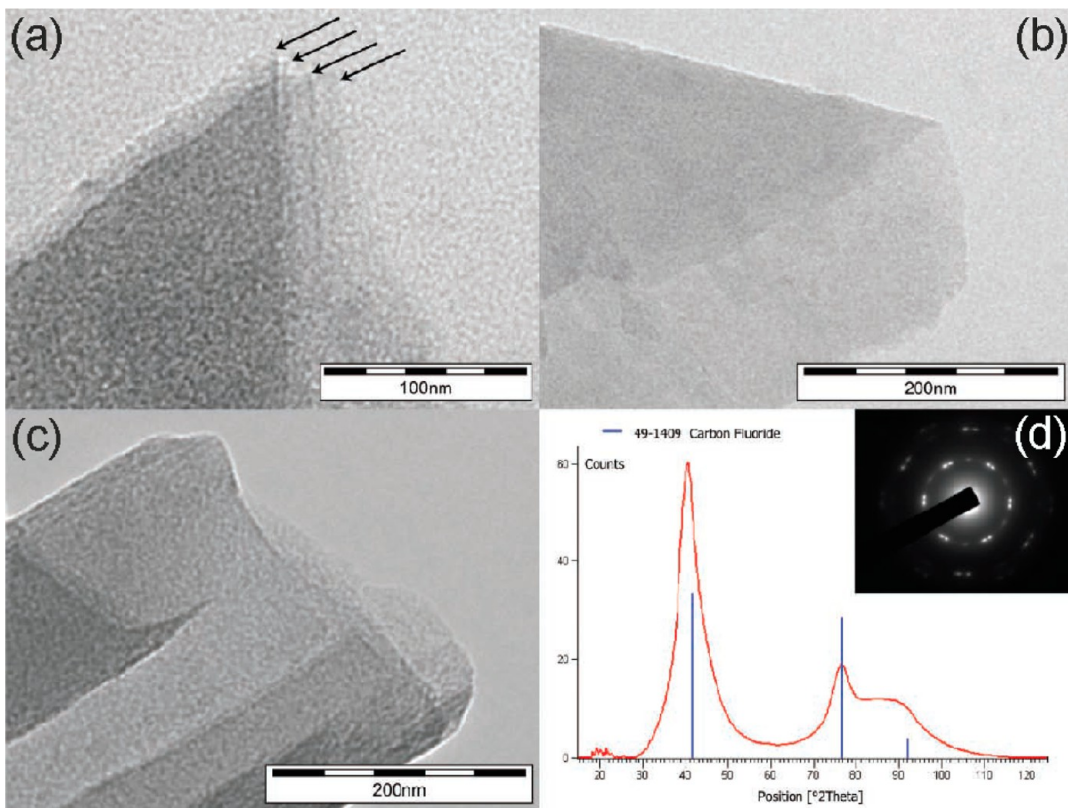


Figure 6. (a,c) Transmission electron microscopy (TEM) images of CF sheets obtained after graphite fluoride exfoliation in sulfolane. (b) Arrows in the HRTEM image indicate highly transparent graphene fluoride monolayers. (d) The selected area electron diffraction (SAED) pattern confirms the stoichiometry and structure of the layers corresponding to the original graphite fluoride. Reprinted with permission from ref 13. Copyright 2010 Wiley.

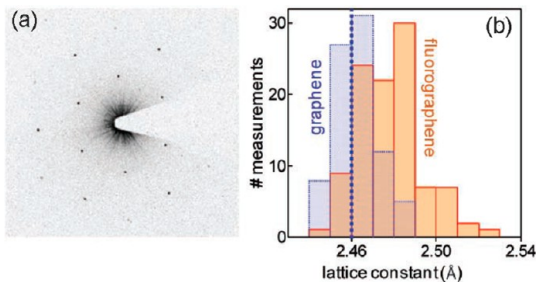


Figure 7. Transmission electron microscopy of CF sheets obtained from graphene exposed to atomic F. (a) Diffraction pattern from a CF membrane. (b) Lattice constant d measured using microscopy images, such as that shown in panel a. For comparison, similar measurements were taken for membranes before fluorination (left histogram). The dotted line indicates d for graphite. Reprinted with permission from ref 12. Copyright 2010 Wiley.

with a nearly gate-independent resistance greater than $1\text{ G}\Omega$, suggesting the presence of a band gap (which is also expected because of the sp^3 carbon net, Figure 1).^{12,14,17} Devices fabricated from fully fluorinated graphene showed no leakage current at biases up to 10 V. The possibility of fabricating a transistor structure using fluorinated monolayer graphene has also been demonstrated.¹⁴ Fluorination has been shown to cause a considerable increase in the resistance in the electro-neutrality region owing to the creation of a mobility gap

in the electronic spectrum where electron transport occurs through localized states.

The density of states of fluorographene has been investigated by near edge X-ray absorption spectroscopy (NEXAFS).³¹ Pure graphene showed peaks at 285.5 and 291.5 eV, corresponding to transitions to the π^* and σ^* conduction states, respectively. The π^* feature (characteristic of sp^2 bonding) gradually decreased with increasing fluorination, providing direct evidence of the formation of sp^3 bonds in fluorographene (Figure 9). A broader hump at 288.4 eV was interpreted as the fluorographene conduction band edge and a much sharper peak at 287.4 eV was attributed to an exciton absorption line. The change in energy difference between the leading edges of the NEXAFS spectra (dashed lines in Figure 9) and the corresponding C 1s core level binding energies of pure graphene and fluorographene, a lower limit of 3.8 eV was estimated for the fluorographene band gap.³¹ We note that for partially fluorinated graphene ($\text{CF}_{0.25}$) a band gap of 2.9 eV was obtained from dI/dV measurement.⁶⁰

Theoretical predictions of the electronic properties of fluorographene have mainly focused on the band structure, namely band gap. Despite extensive research efforts, questions remain regarding the band structure of fluorographene.⁵⁹ The band gap is usually

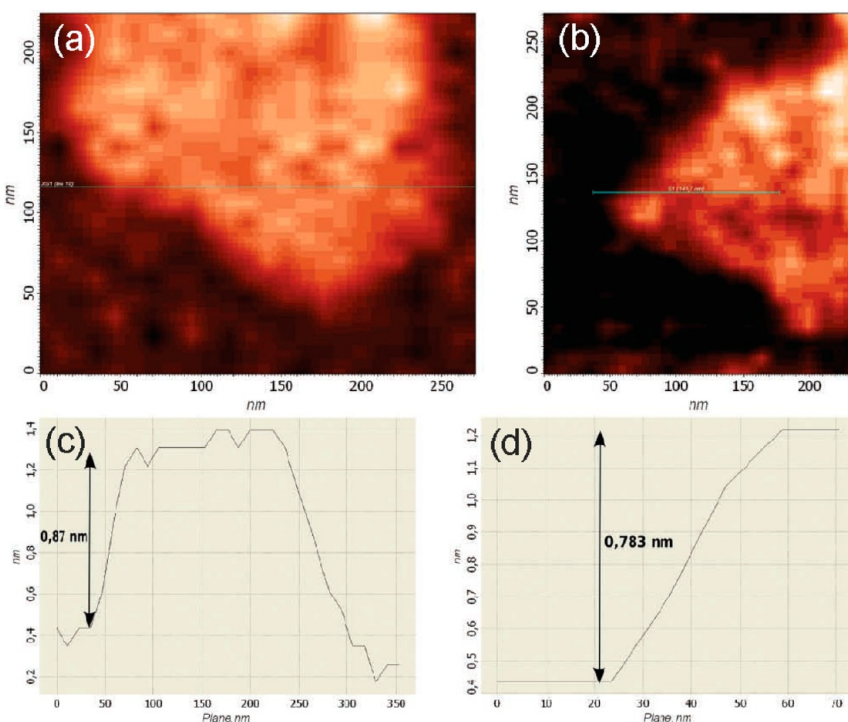


Figure 8. (a,b) Two independent AFM images of graphene fluoride monolayers and (c,d) their height profiles, providing evidence that the layers are <0.9 nm thick. Reprinted with permission from ref 13. Copyright 2010 Wiley.

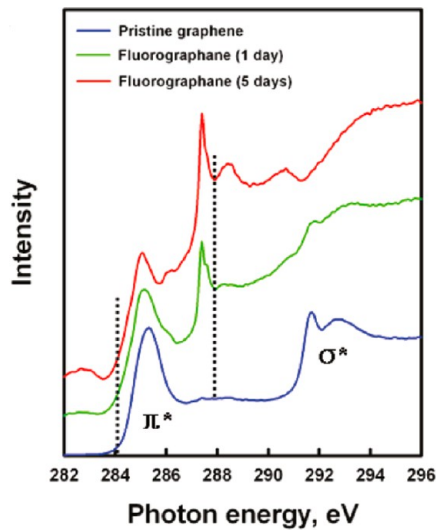


Figure 9. NEXAFS spectra of pristine graphene and fluorographene with two different fluorine contents. The dashed lines at 284.1 and 287.9 eV mark the leading edges of the π^* resonance for the pristine and fluorinated sample, respectively. Reprinted from ref 31. Copyright 2011 American Chemical Society.

considered for the chair conformation of fluorographene with a unit cell containing four atoms (see Figure 5 showing the unit cell and Brillouin zone). Traditional local density approximation (LDA) or generalized gradient approximation (GGA) to DFT predicts that fluorographene is a direct band gap material: the bottom of the conduction band and top of the valence band are located at the Γ point in the first Brillouin zone

(Figure 10). The top of the valence band is doubly degenerate and the maximum band gap is located at the K points. The minimal direct band gap of fluorographene of about 3.1 eV^{53,56–59,61–63} predicted from GGA DFT indicates that fluorographene possesses insulating properties, in agreement with early calculations on graphite fluoride.^{50,64} Band gap values of other fluorographene conformations (Figure 4) are rather similar or slightly higher up to 4.2 eV for the armchair configuration.^{53,54} However, one main limitation of the DFT approach is it is an inherently ground-state theory. LDA and GGA functionals systematically underestimate Kohn–Sham band gaps (compared to experimentally determined values), whereas the Hartree–Fock method systematically overestimates them. Hybrid functionals contain a fraction of Hartree–Fock exchange, and their computationally accessible short-range variants (as by Heyd, Scuseria, and Ernzerhof (HSE)⁶⁵) are often effective for predicting band gaps of solids and low-dimensional carbon materials;⁶⁶ the HSE06 functional⁶⁷ predicts a band gap of about 5 eV for fluorographene.⁵⁸ The high-level many-body GW approximation (GWA), which includes electron–electron interactions beyond DFT, predicts a band gap of 7.0–8.3 eV^{53,54,56,59,68–70} (depending on GW level and orbitals used),⁵⁹ that is, around two times larger than the value obtained with GGA DFT (Figure 10). Any agreement between GGA DFT and experimental “optical band gap” values (>3.0 or >3.8 eV, see below) is coincidental. On the other hand, accurate GW electronic band gaps and the energies of electron

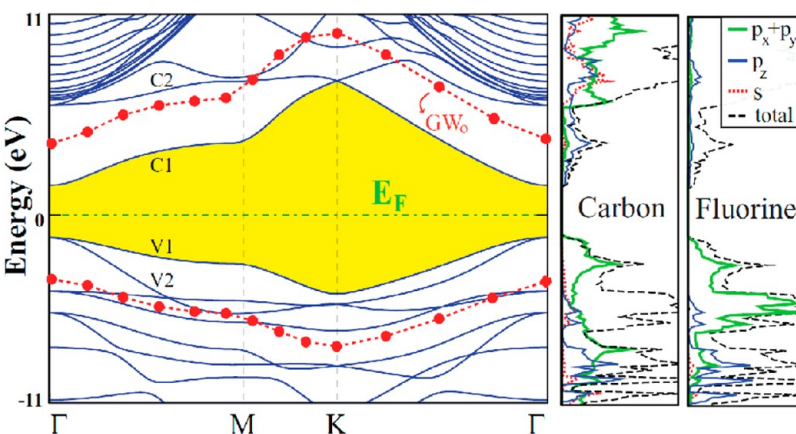


Figure 10. Band structure of CF, together with the orbital PDOS and total DOS. The LDA band gap is shaded and zero energy is set to the Fermi level, E_F . Valence and conduction band edges after GW_0 correction are indicated by filled (red) circles. Reprinted with permission from ref 69. Copyright 2011 American Physical Society.

transitions derived from optical spectra do not exactly match each other, because the electron transitions observed in optical spectra involve formation of an exciton. Therefore DFT and GW band gaps should not be directly compared with absorption peaks in optical spectra and reasonable agreement with optical measurement can be achieved only after inclusion of electron–hole correlations into calculations (see below for BSE–GWA spectra).^{59,70} Effect of various defects on discussed electronic properties is probably rather small.⁵⁹ GWA predicts that the band gap of fluorographene is greater than that of graphane, whereas GGA functionals suggest the opposite trend. Recent calculations have shown that it is possible to obtain the same order of band gaps with DFT as from GW if the screened hybrid functional HSE06 is used.^{58,59}

Recently, spin–orbit couplings (SOCs) of fluorographene have been calculated by DFT.⁶¹ The results suggested that SOC-induced band splittings near their Fermi energies in fluorographene are significantly higher (of the order of 10^{-2} eV) than for pure graphene (of the order of 10^{-6} eV) and are comparable to values for diamond and archetypal semiconductors.⁶¹

Optical Properties of CF. Studies of the absorption spectra of pristine, partially fluorinated or fully fluorinated graphene have revealed that they exhibit dramatically different optical properties (Figure 11). Graphene shows an absorption spectrum that is relatively flat for light energies <2.5 eV but which strongly increases in the blue light region and has an absorption peak in the ultraviolet range (4.6 eV). In comparison, partially fluorinated graphene shows higher transparency, whereas fluorographene appears to be transparent at visible frequencies and only starts absorbing light in the blue region (Figure 11).¹² This proves that fluorographene is a wide-gap semiconductor or insulator with band gap ≥ 3.0 eV. Further, the absence of Raman signatures confirms (virtually no sp^2 coordinated carbon remains; see section 3.4. below) the

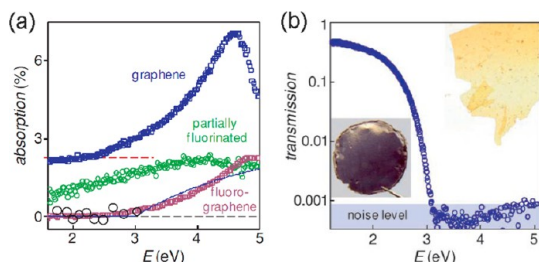


Figure 11. (a) Changes in optical transparency of graphene due to fluorination. The solid curve is the absorption behavior expected for a 2D semiconductor with band gap of 3 eV. (b) Graphene paper before and after fluorination (left and right insets, respectively). The plot shows the optical transparency of fluorographene paper as a function of energy for a sample of 1 cm size and 5 μm thick in the photograph. Reprinted with permission from ref 12. Copyright 2010 Wiley.

complete optical transparency of fully fluorinated graphene.¹² Nair *et al.*¹² have also studied fluorinated graphene laminates of macroscopic size (Figure 11). This material was found to be optically transparent with a yellowish color that corresponds to absorption in the violet region. This provides direct visual evidence that fluorographene is a wide-gap material. The light transmission spectra exhibited an onset at ~ 3.1 eV, in agreement with the gap value obtained from the absorption spectra of individual fluorographene crystals.¹²

Photoluminescence measurements of fluorographene dispersion in acetone have shown emission peaks at 3.8 and 3.65 eV (Figure 12).³¹ The former peak has been assigned to band-to-band recombination of free electrons and holes because the same energy was measured for the band gap of fluorographene by NEXAFS. The 3.645 eV peak was 156 meV (1260 cm^{-1}) below the band gap emission, corresponding to the C–F vibration mode. This feature was attributed to phonon-assisted radiative recombination across the band gap, for which the C–F vibration mode is excited when the electron–hole pair recombines. With a lower degree of

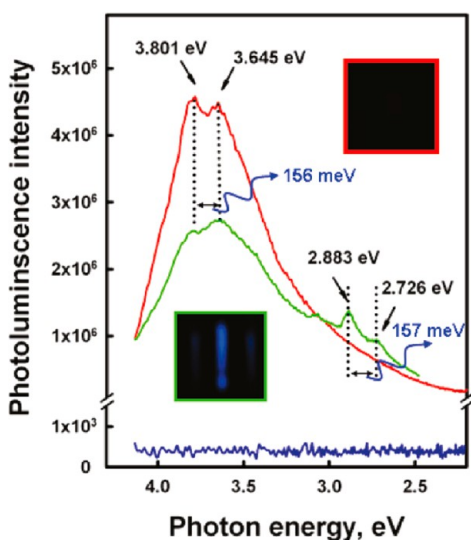


Figure 12. Photoluminescence emission spectra recorded at room temperature (excitation at 290 nm, 4.275 eV) of graphene (blue) and fluorographene (green, 1 day fluorination; red, 5 days). Reprinted from ref 31. Copyright 2011 American Chemical Society.

fluorination (1 day of fluorination), an additional emission peak at 2.88 eV was observed, which was also accompanied by a second peak located 157 meV (Figure 12). The optical band gap of fluorographene is nearly 3.8 eV, wide enough for optoelectronic applications in the blue/UV region.³¹

The first exciton peaks in the fluorographene absorption spectrum have been predicted theoretically using Bethe-Salpeter equation (BSE) on top of GWA, which accounts for electron–electron (e–e) and electron–hole (e–h) correlations, and compared with spectra from the random-phase approximation (RPA) on top of GWA (without e–h).^{54,59,68,70} For the single-particle result (Figure 13a, the blue curve, without e–h) the onset of the spectrum was located at the GWA band gap and the absorption profile increased very slowly until near 10 eV. This was interpreted as small spatial overlapping of the wave functions of the valence band maximum (VBM) and the conduction band minimum (CBM), implying that the lowest optical transition from VBM to the CBM (Figure 13b, transition v1–c1) is weak. The notable optical absorption starting from 10 eV was mainly attributed to transitions from high energy valence bands to the second conduction bands with energies varying from 8 to 11 eV (Figure 13b, transition v1–c2). When e–h interactions were taken into account, a prominent peak was observed, which originated from a few strong resonant excitonic states that appeared at 9–10 eV^{54,59,68,70} (Figure 13a). The major contribution to this feature was related to transitions from the top two valence bands and the lowest four conduction bands (Figure 13b, two dominant transitions v1–c2 and v2–c1). In the low-frequency optical absorption spectrum, a bound exciton at 3.8 eV

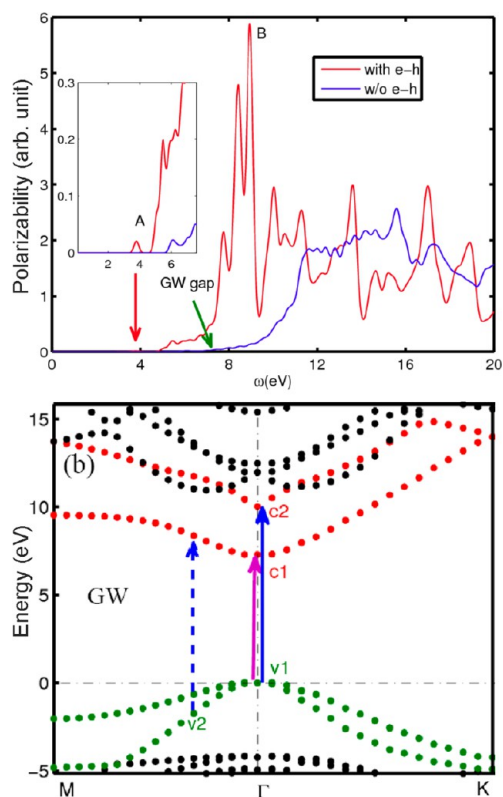


Figure 13. (a) Optical absorption spectra of fluorographene with (red line, BSE-GWA) or without e–h interactions (blue line, RPA-GWA). (b) GW band structure of fluorographene. Reprinted with permission from ref 68. Copyright 2011 The Materials Research Society.

(or alternatively 5.4 eV⁵⁴ and 5.1 eV^{59,70}) was identified with a huge binding energy of 3.5 eV (or alternatively 2 eV) and comparatively weak optical activity (inset of Figure 13a). The large occupation probability associated with the low energy of this excitonic state suggests it might play a vital role in the photoluminescence of this material and explains the prominent ultraviolet luminescence peak reported experimentally by Jeon *et al.*³¹

Vibrational Properties of CF. Theoretical analysis of vibrational modes can provide valuable insights into the experimental Raman and infrared spectra of fluorographene CF. In particular, since Raman spectra convey information on a particular structure, and hence can be viewed as its signature, observed peaks are compared to the calculated Raman-active modes. Theoretical analysis has revealed that the phonon spectra and density of states (DOS) of the most stable chair conformation do not show clearly separated groups of phonons (Figure 14). The dominant contribution to the acoustic modes has been attributed to the fluorine atoms, whereas the high-frequency modes around 1200 cm^{-1} have a clear carbon character.⁷¹ Twelve phonon modes of the chair conformation of fluorographene, which has $P\bar{3}m1$ symmetry (D_{3d} point group), have been shown to belong to four irreducible representations: E_g and A_{1g} are Raman active modes,

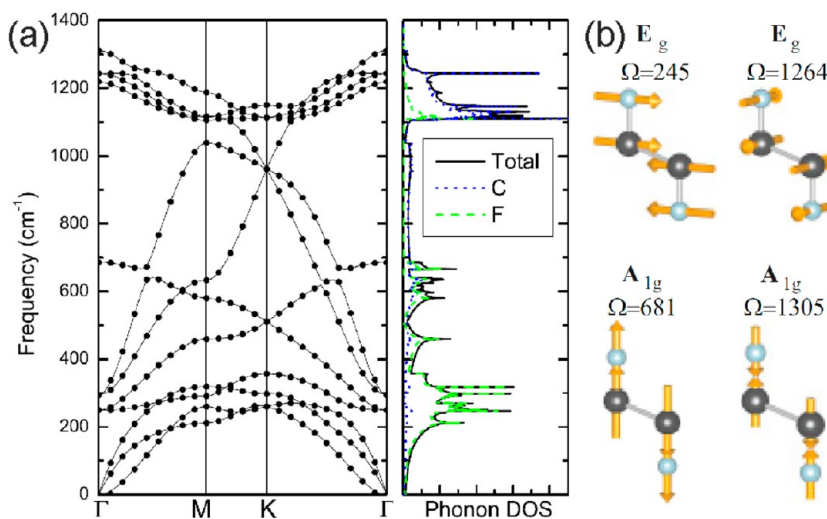


Figure 14. (a) Phonon dispersion of CF in the chair conformation and the corresponding phonon DOS. Reprinted with permission from ref 71. Copyright 2011 American Institute of Physics. (b) Symmetries, frequencies, and descriptions of Raman-active modes of CF. Reprinted with permission from ref 69. Copyright 2011 American Physical Society.

while E_u and A_{2u} are infrared active modes (Table 1). Some of the phonon branches of the CF boat conformation have imaginary frequencies, and hence it is predicted to be unstable in spite of the fact that such a structure can be optimized.⁶⁹ However, the possibility that this unstable structure can occur at finite and small sizes cannot be excluded.

Because Raman spectroscopy provides a wealth of useful information, it has been actively used during the fluorination process of graphene (Figure 15).^{12,14,16,17} However, because the energies of the lasers used were lower than the band gap (fluorographene is wide band gap material), no signature Raman activity from fully fluorinated regions was observed in those experiments^{12,14,16} and the only Raman peaks were associated with graphene. The main features in the Raman spectra of pristine graphene are the G- and 2D-bands, which occur around 1580 and 2680 cm^{-1} , respectively (Figure 15). The G-band is associated with the doubly degenerate E_{2g} phonon mode of graphene, whereas the 2D mode (also called G') originates from a second-order process, involving two phonons near the K point without the presence of any kind of disorders or defects. Conversely, the presence of defects in the sample activates additional peaks in the Raman spectra of graphene. The D, D', and D+D' peaks involve phonon modes from graphene, and hence occur at the same frequencies in partially fluorinated samples (at 1350, 1620, and 2950 cm^{-1} , respectively; Figure 15a).^{12,14,16} These Raman peaks originate from double resonance processes at the K point in the presence of defects. The D and G peaks of graphene provide valuable information on the density of defects. These peaks disappear for almost fully covered samples, which has been found for fluorographene^{12,14,16} but not in previous experiments on graphane or graphite fluorides.

TABLE 1. List of Symmetries and Phonon Frequencies at Different k -points for Fluorographene. R and I Indicate Raman and Infrared Active Modes, Respectively⁷¹

symmetry (activity)	Γ	M	K
A_{2u} (R)	0	211	260
E_u (I)	0	260	260
E_u (I)	0	291	298
E_g (R)	250	318	356
E_g (R)	250	459	510
E_u (I)	294	580	510
E_u (I)	294	633	961
A_{1g} (R)	686	1039	962
E_g (R)	1244	1106	962
E_g (R)	1244	1116	1114
A_{2u} (I)	1219	1117	1114
A_{1g} (R)	1312	1188	1150

The first report on Raman signatures of CF in the low-frequency region by using a UV laser (with energy of 5.08 eV) was by Wang *et al.*¹⁸ Two Raman active modes were detected at 1270 and 1345 cm^{-1} , which are absent under lower laser energies. Even though the CF samples also contained multilayer regions, the experimental values correlated with the aforementioned DFT phonon frequencies (Figure 14): the higher-frequency mode as A_{1g} mode with out-of-plane motions of F against C (at 1312 or 1305 cm^{-1})^{69,71} and the lower-frequency mode as a 2-fold degenerate in-plane E_g vibration (at 1244 or 1264 cm^{-1}).^{69,71}

FTIR spectra obtained in transmission mode (Figure 16a) have shown that fluorographene exhibits much stronger IR bands than graphene due to the greater transparency of the former.³¹ Furthermore, a prominent feature at 1260 cm^{-1} characteristic of covalent C–F bond stretching⁷² has been observed. For fluorographene exfoliated by *N*-methyl-2-pyrrolidone (NMP), peaks at 1212 and 1084 cm^{-1} were observed

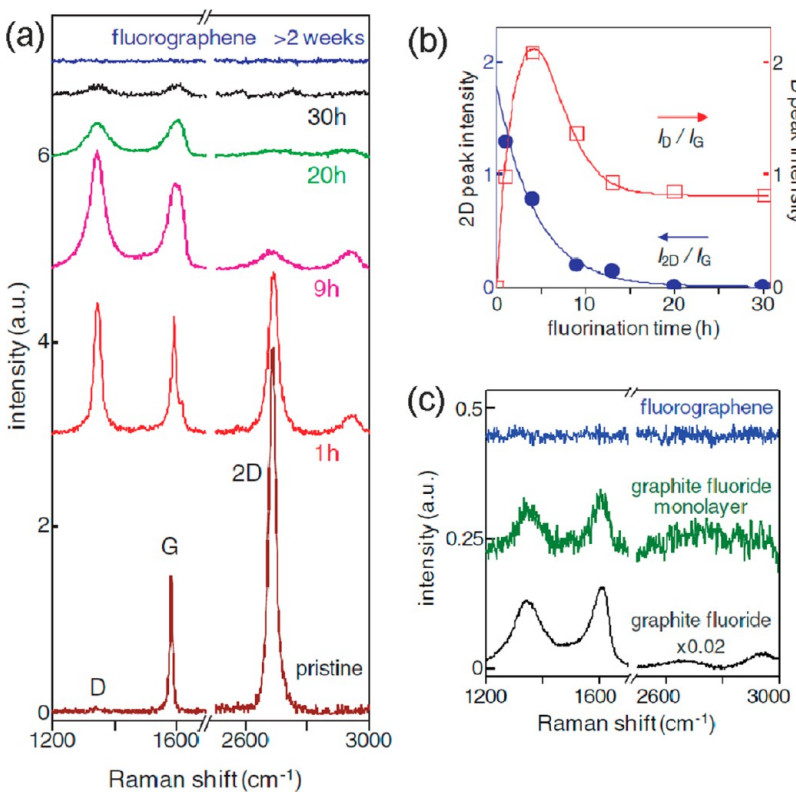


Figure 15. Raman signatures of CF. (a) Evolution of the spectra for a graphene membrane exposed to atomic F and measured as a function of time under the same Raman conditions. The curves are shifted for clarity. (b) Intensities of the D and 2D peaks (normalized with respect to the G peak intensity) as a function of fluorination time. The solid curves are for guidance only. (c) Comparison of CF membranes with graphite fluoride and its monolayer. Reprinted with permission from ref 12. Copyright 2010 Wiley.

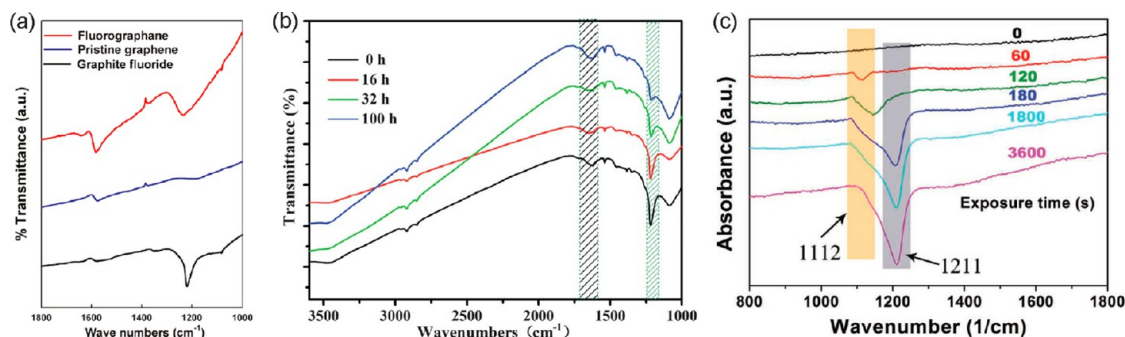


Figure 16. (a) FTIR spectra of CF prepared by fluorinating graphene, pristine graphene, and graphite fluoride. Reprinted from ref 31. Copyright 2011 American Chemical Society. (b) FTIR spectra of CF obtained at different sonication times for graphite fluoride exfoliated by NMP. Reprinted with permission from ref 23. Copyright 2012 Royal Society of Chemistry. (c) Evolution of CF phases on graphene with increasing exposure time to XeF_2 characterized by FTIR spectra. Reprinted with permission from ref 31. Copyright 2012 Wiley.

corresponding to the stretching vibration of the C—F covalent bonds and the semi-ionic stretching vibration of C—F bonds, respectively (Figure 16b).²³ Studies of FTIR spectra with increasing fluorination time (Figure 16c) have revealed an absorption band at 1112 cm^{-1} related to the 'semi-ionic' C—F, which gradually changes into a strong band at 1211 cm^{-1} attributable to covalent C—F bonding.⁷³ An experimental infrared active mode at 1204 cm^{-1} has also been reported.¹⁸ The aforementioned frequencies of the experimental infrared active mode corresponding to C—F stretching agree with the

calculated infrared active mode A_{2u} at the Γ point (at 1219 cm^{-1} , Table 1).⁷¹

The experimental determination of the phonon dispersion relations of fluorographene can be very useful in the characterization of this material. As fluorographene is a wide band gap material, this allows discrimination of the Raman activity originating from the fully fluorinated regions during synthesis by using a laser with appropriate energies.⁷¹

Mechanical, Thermodynamical Properties and Stability of CF. Graphene and its derivatives graphane and

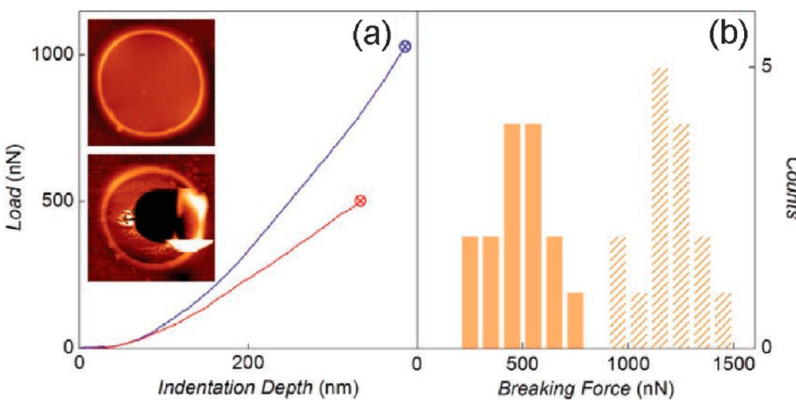


Figure 17. Mechanical properties of CF. (a) Examples of the loading curves for graphene (blue) and CF (red) membranes. Fracture loads are marked by the circled crosses. Up until these breaking points, the curves were nonhysteretic. Top and bottom insets: AFM images of a CF membrane before and after its fracture, respectively. (b) Histogram of the breaking force for graphene (hatched) and CF (solid color). All the membranes (15 of each type) were mounted on identical Quantifoils and contacted with the same AFM tip. Reprinted with permission from ref 12. Copyright 2010 Wiley.

fluorographene can be isolated and made into free-hanging membranes. This makes it possible to measure the elastic constants of these materials from nanoindentation experiments by an atomic force microscope. The experimental elastic constants can be compared to first-principles calculations, giving information about the purity and structural crystallinity of the experimental samples. Nair *et al.*¹² have conducted a nanoindentation experiment on fluorographene by recording the bending of an AFM cantilever as a function of its displacement, and hence calculated the force acting on the membrane (typical loading curves and breaking forces are shown in Figure 17), giving a value of $100 \pm 30 \text{ N m}^{-1}$ or 0.3 TPa for the 2D Young's modulus, (three times less stiff than graphene due to the longer sp^3 type bonds in CF). However, the experimental Young's modulus was approximately half the theoretical value (226 N m^{-1}).⁵³ This was attributed to an appreciable number of defects in the experimental samples. Large scale atomistic simulations using the reactive force field approach have shown⁷⁴ that fluorographene remains a flat sheet (unrippled) similar to graphane even at high temperature, that is, up to 900 K , in contrast to the thermal rippling behavior of graphene.

The variation of the strain energy, E_s , and its derivative with respect to the applied uniform strain, $dE_s/d\varepsilon$, have been predicted theoretically (Figure 18a; comparison with CH and CCl).⁷⁵ The results showed that the derivative was linear for small ε in the harmonic range. Elastic deformation continued until the maximum of $dE_s/d\varepsilon$, whereupon the structure reverted to its initial state when the applied strain was lifted. Beyond the maximum the structural instability sets in with irreversible deformations. The region beyond the maximum is called the plastic region. The effect of elastic strain on the band gap of CCl, CF, and CH was also calculated, and the results are presented in Figure 18b. CH and CCl were predicted to have similar

response to elastic strain: their band gaps increased for small strain followed by a rapid decrease for large strain. In contrast, the band gap of CF did not initially show any significant increase with increasing strain: for small strain it was almost unaltered, but decreased rapidly for large strain.

Superior nanoscale friction on fluorinated graphene has been reported by Park *et al.*^{60,76} using ultrahigh vacuum friction force microscopy. The measured friction on fluorinated graphene with C_4F composition was ~ 6 times larger than on pure graphene for applied normal forces up to 150 nN , whereas fluorination slightly reduced (by about 25%) the adhesion force between the AFM tip and graphene.⁶⁰ DFT calculations confirmed reduction of the adhesive properties and showed friction force on graphene mainly governed by out-of-plane bending.⁷⁶ In contrast, low interlayer friction was reported for multilayer CF from dispersion corrected DFT calculations.⁷⁷

Electrical measurements (Figure 19) have been utilized to study the thermal stability of CF in more detail than possible with Raman spectroscopy.¹² The thermal stability of CF was observed to be higher than that of graphene, graphene oxide, and even graphite fluoride. Under similar conditions, graphite fluoride began decomposing at $300 \text{ }^\circ\text{C}$. The higher stability of CF can be due to the absence of structural defects and strain. The thermal stability and chemical inertness of CF was comparable to that of the fully fluorinated 1D carbon chain of Teflon.^{12,23} CF underwent slow decomposition at $T > 260 \text{ }^\circ\text{C}$ and rapidly decomposed only above $400 \text{ }^\circ\text{C}$. These properties in principle make colloidal CF derived from graphite fluoride a favorable candidate to replace Teflon in various protective coatings. CF has also been shown to be resistant to various solvents under ambient conditions.

Chemistry of CF and Applications. Hydrophobic graphene fluoride ($\text{CF}_{0.5}$) nanosheets can be made water dispersible by stabilizing them with fluoro-surfactants.

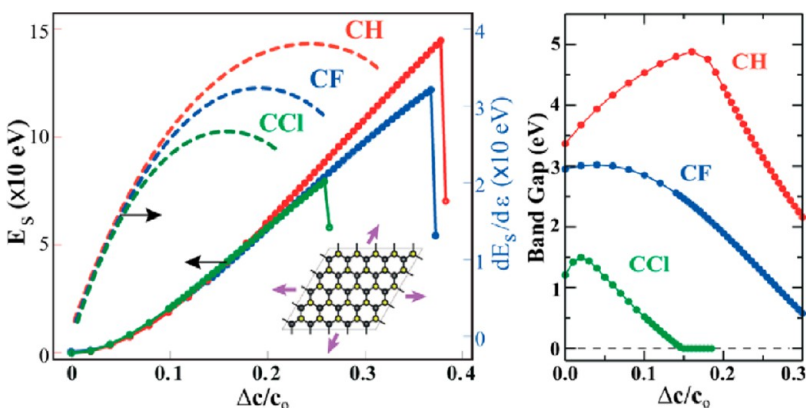
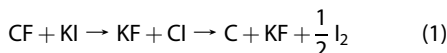


Figure 18. (a) Variation of the strain energy E_s (curves on the righthand side) and its derivative with respect to applied uniform strain ε , i.e., $dE_s/d\varepsilon$ (curves on the left-hand side) calculated for CCl, CH, and CF. After the maxima, these structures become unstable and undergo plastic deformation. (b) Variation of the band gap with uniform strain. Reprinted from ref 75. Copyright 2012 American Chemical Society.

Recently, our group reported nonlinear optical response of graphene fluoride *via* aqueous phase exfoliation of graphite fluoride with the aid of a fluorosurfactant.⁷⁸

The fluorination process is reversible as fluorine can be easily removed from CF by thermally annealing the sample (defluorination) in the presence of hydrogen gas or anhydrous hydrazine vapor. Robinson and co-workers have shown that chemical reduction of fluorographenes by means of hydrazine vapor is more effective for defluorination than thermal annealing *via* Raman spectroscopy.¹⁶ Thermal defluorination (400–600 °C) of graphene fluoride has been shown to result in the removal of carbons and evolution of C–F products (e.g., CF_4 , C_2F_4 , C_2F_6).^{16,79}

The addition of KI to a colloidal CF dispersion forming graphene is also an interesting approach for defluorination.¹³ In this reaction CF transforms into unstable graphene iodine (iodographene), which rapidly disproportionates into graphene and iodine:



The structure and electronic properties of fluorographene doped with metals such as K, Li, Au atoms and $C_{12}N_4F_4$ (F4-TCNQ) have been investigated by density functional theory. It was shown that adsorption of K or Li atoms results in the electron doping of fluorographene, whereas Au atoms and F4-TCNQ introduce deep levels inside the band gap.⁸⁰

Furthermore, the strong polarity of the C–F bonds stimulates interesting biological responses. Wang and co-workers⁷³ observed that bone marrow derived mesenchymal stem cells (MSCs) cultured on fully fluorinated graphene proliferated faster and were more confluent after a week than cells cultured on partially fluorinated graphene and graphene (Figure 20a–c and Figure 20d). The fully fluorinated graphene was associated with a nearly 3-fold increase in cell density, showing that the introduction of C–F bonds on the surface of graphene facilitates cell adhesion and

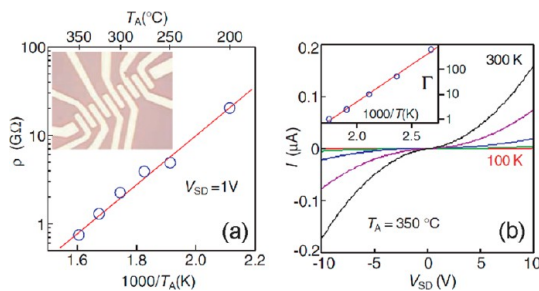


Figure 19. Characteristics of highly stable 2D insulator. (a) Changes in fluorographene's resistivity ρ induced by annealing. No changes were detected at T_A below 200 °C. At higher T_A , ρ decreased below 1 TΩ and was experimentally measurable. Owing to nonlinear I – V characteristics, the plotted ρ values were recorded for a fixed bias V_{SD} of 1 V (circles). For any given T_A , approximately 1 h was required to reach a saturated state. The solid line shows the exponential dependence yielding $E_{des} \approx 0.65$ eV. (b) I – V characteristics for partially fluorinated graphene obtained by reduction at 350 °C. The curves from flattest to steepest were measured at $T = 100, 150, 200, 250$, and 300 K, respectively. The scaling factor Γ is plotted in the inset. The solid line shows the best fit to the function $\exp(E_h/T)$. Reprinted with permission from ref 12. Copyright 2010 Wiley.

proliferation. To understand the effect of texture and wettability on the controlled growth of MSCs on the surface fluorinated graphenes, water contact angle measurements were performed. The surface roughness of the graphene increased with increasing fluorine content, thereby reducing the water contact angle from 83 to ~1° (graphene to fully fluorinated graphene; the insets in Figure 20e–g). In addition, selective attachment of MSCs over microchannels of CF was achieved *via* patterning CF with PDMS. This work opens up interesting avenues for partially and fully fluorinated graphenes in tissue engineering related applications.

Quantum Monte Carlo simulations predicted qualitative different behavior of helium films on fluorographene and graphane with respect to behavior on graphite because of the different surface composition, symmetry, and spacing of the adsorption sites.⁸¹ The commensurate state analogous to the $\sqrt{3} \times \sqrt{3} R30^\circ$

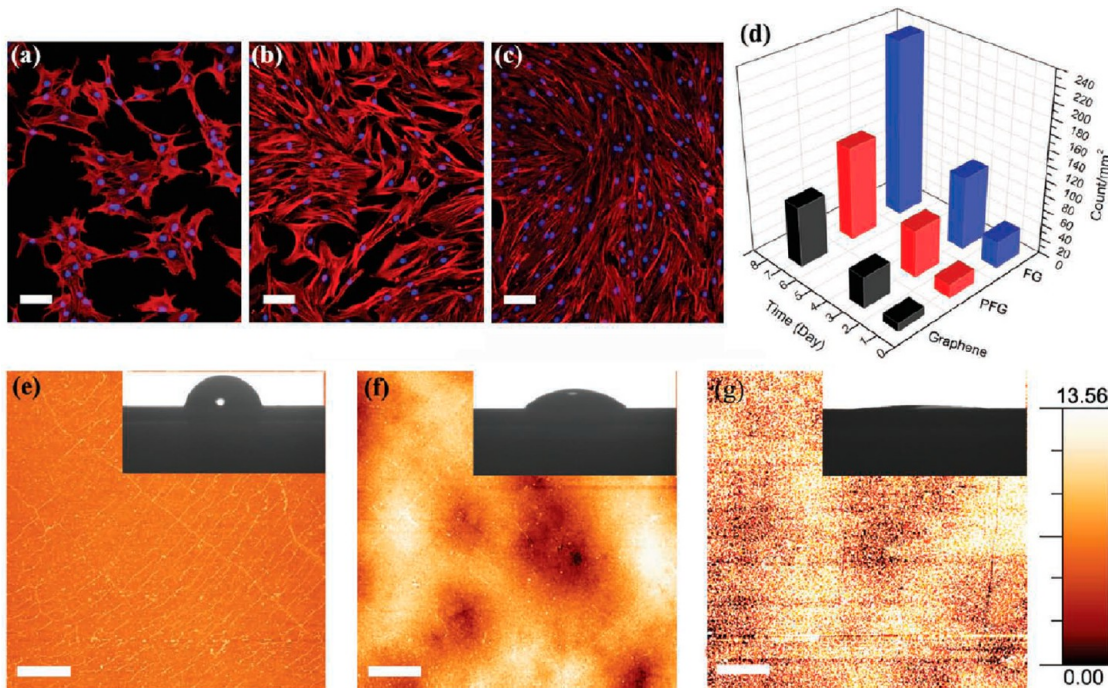


Figure 20. (a–c) Fluorescent images of the actin cytoskeleton of MSCs cultured on graphene, partially fluorinated graphene or fluorographene stained with rhodamine–phalloidin on day 7 (scale bar = 100 μm). (d) Proliferation of MSCs cultured on the graphene films, showing the controlled growth of MSCs on fluorinated graphene with different coverage of fluorine. (e–g) AFM images of graphene, partially fluorinated graphene, and fluorographene, respectively, showing the surface of fluorinated graphene (scale bar = 5 μm). The insets show data for the water contact angle. Reprinted with permission from ref 73. Copyright 2012 Wiley.

on graphite was unstable, while a superfluid ground state for ^4He and a fluid ground state for ^3He were found on fluorographene and graphene.

Fluorinated Graphenes. *Basic Properties of Partially Fluorinated Graphenes (C_1F_n , $n < 1$).* The introduction of fluorine modifies the electronic properties of graphene by reducing the charge in the conducting π orbitals.^{16,17} The resistance of the fluorinated graphenes can be tuned by the extent of fluorine content. For example, fluorinated graphene with a composition of $\text{CF}_{0.25}$ has been shown to have a 6-fold higher resistance than pristine graphene; in addition, $\text{CF}_{0.25}$ has been shown to be a wide band gap material that exhibits optical transparency.¹⁶ Furthermore, defluorination of these samples either by heating or exposing to hydrazine vapors restored the conductivity and the ambipolar nature similar to that of graphenes. For various applications related to the fabrication of devices, single-side fluorination of graphene would be sufficient as it opens a significant band gap.²⁰ Single-side fluorination can easily lead to a random surface coverage of up to $\text{CF}_{0.5}$.⁸² Band gaps of fluorinated graphenes (obtained by exfoliating graphite fluoride *via* fluorinated ionic liquids) with compositions $\text{CF}_{0.25}$ and $\text{CF}_{0.5}$ have been measured by diffuse reflectance spectroscopy as nearly 1.8 and 2.2 eV, respectively;¹⁹ however, a band gap of 2.9 eV was obtained from dI/dV measurement on $\text{CF}_{0.25}$ (XeF_2 fluorination of CVD graphene as grown on a copper foil).⁶⁰

From the theory, the most stable single-side conformation of C_1F_a , where $a < 1$, is predicted to be $\text{CF}_{0.25}$.¹⁶ Density of states calculations for graphene with increasing F coverage showed widening of the band gap and lowering of the Fermi level in the valence band.¹⁶ Tuning the band gap (*ca.* 0–3 eV at DFT level) can be achieved by precise adsorption of fluorine as well as a transformation from nonmagnetic semimetal (graphene) to either a nonmagnetic/magnetic metal or a magnetic/nonmagnetic semiconductor/insulator with a direct band gap.⁸³ Band gaps of 2.93 eV (LDA) or 5.99 eV (GW_0) for $\text{CF}_{0.25}$ and 1.57 eV (LDA) or 5.68 eV (GW_0) for boat $\text{CF}_{0.5}$ have been predicted (Figure 21a–c).⁶⁹ In theoretical studies, the total energies and/or binding energies have often been used as criteria for whether a given CF_n structure exists. Even if a CF_n structure seems to be in a minimum on the potential energy surface, its stability should be meticulously examined by calculating frequencies of all phonon modes in the Brillouin zone (BZ). Sahin *et al.*⁶⁹ found that the $\text{CF}_{0.25}$, the $\text{CF}_{0.5}$ boat, and the $\text{CF}_{0.5}$ chair structures have positive frequencies throughout the BZ, indicating their stability. Optical absorption spectra of $\text{CF}_{0.25}$ calculated from Bethe-Salpeter equation (BSE) have shown strong excitonic effects (analogically with CF, see subsection “Optical properties of CF” above).⁷⁰ The first exciton peak locates at 4.21 eV (Figure 21d, black line); that is, the onset of absorption spectra is significantly shifted to lower energies with respect to

electronic GW band gap (6 eV⁶⁹ from GW_0 , 5.5 eV⁷⁰ from G_0W_0). It is worth noting that large scale molecular dynamics simulations have shown a rolling of graphene as a consequence of strain when graphene is fluorinated/hydrogenated from a single side.⁸⁴ Therefore, in the absence of a substrate, free-standing single-sided halogenated graphene will not be a flat atomic layer.

Recently, fluorinated graphene obtained by cooperative exfoliation of graphite fluoride using cetyl-trimethyl-ammonium bromide (CTAB) and dopamine have been shown to exhibit a full-color emission from violet to red light (3.10–1.65 eV) when excited at 365 nm.²⁴ Band gap energies of fluorinated graphene (however, containing also oxygen) for several fluorine coverages have been measured (Figure 22).²¹ There is a blue shift observed for the fluorinated graphene sheets as compared to that of graphene sheets (*i.e.*, from 269 nm of graphene to 251 and 247 nm in Figure 22a) indicating the opening of the band gap. Moreover, the higher coverage of fluorine in graphene sheets decreases the electrical conductivity (Figure 22b) and band gap widening (from 1.8 to 2.9 eV for $CF_{0.10}$ and $CF_{0.48}$, respectively) was observed (Figure 22c,d).

Fluorine-doped reduced graphene oxide (RGO) is reportedly a better substrate for surface enhanced Raman spectroscopy of molecules than unmodified RGO.³³ In addition, it has been shown that the chemical enhancement factor can be tuned by changing the fluorine/carbon ratio (17–27 atom %) due to the presence of a strong local electric field induced by the local dipoles of F-containing groups on the RGO surface.³³ Thomas *et al.*⁸⁵ have reported that fluorinated graphene oxide has high nonlinear absorption and nonlinear scattering, and its optical limiting threshold is about an order of magnitude better than that of graphene oxide (GO).

Raman spectroscopy of fluorinated graphenes has been mainly discussed in the fluorographene section. Single side fluorination leads to the appearance of a D peak at 1350 cm^{-1} and broadening of the G (1580 cm^{-1}) and D' peaks (1620 cm^{-1}), as well as a decrease in the 2D Raman peaks which is similar to that of graphene oxide.¹⁶ Sun and co-workers³⁵ have studied layer-dependent fluorination of n-layer graphenes by SF_6 plasma treatment. They observed that fluorination of monolayer graphenes is easier and faster than multilayer graphenes because of the former's high surface reactivity due to corrugations which become notably smaller for bilayers and disappear for thicker graphenes. During fluorination of monolayer graphene, three new peaks at 1350, 1620, and 2920 cm^{-1} were observed in the Raman spectra, which were ascribed to D, D', and D+G bands, respectively. The presence of D, D', and D+G bands indicates that defects were introduced into the graphene lattice during the plasma treatment, which occurs more easily for single-layer graphene than thicker graphenes. The same group also observed that fluorination by

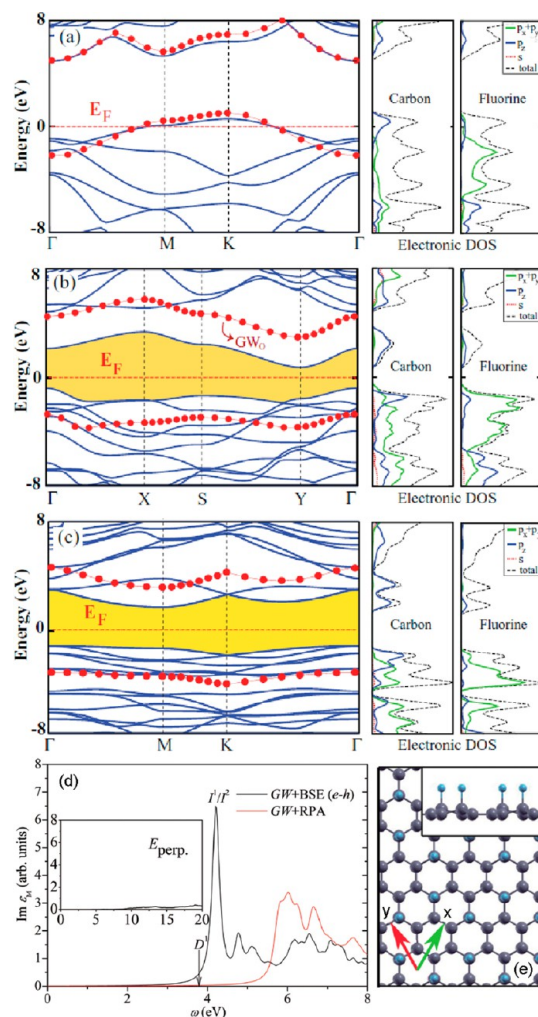


Figure 21. Energy band structures of various stable CF_n structures, together with the orbital partial densities of states (DOS) and total DOS. The LDA band gaps are shaded and zero energy is set to the Fermi level, E_F . The total DOS is scaled to 45%. Valence and conduction-band edges after GW_0 correction are indicated by filled (red) circles. (a) $CF_{0.5}$ chain structure. (b) $CF_{0.5}$ boat structure. (c) $CF_{0.25}$ structure. Reprinted with permission from ref 69. Copyright 2011 American Physical Society. (d) Absorption spectra of C_4F for light parallel to the surface plane (along x direction, see panel e) calculated with and without the consideration of electron–hole Coulomb interaction, that is, $GW+BSE$ and $GW+RPA$, respectively. The inset is the absorption spectrum of C_4F for light polarization perpendicular to the surface plane. Reprinted with permission from ref 70. Copyright 2013 American Physical Society.

CF_4 plasma treatment induces a lower number of lattice defects and higher magnitude of p-doping to graphene than CHF_3 plasma treatment.³⁴

Other Unusual Properties of Fluorinated Graphenes and Applications. Dilute fluorinated graphene sheets (F/C ratio of 1 to 2000 or 0.05%) produced by CF_4 plasma in a reactive ion etching system have been shown to exhibit anisotropic, colossal negative magnetoresistance and unusual “staircase” behavior at low temperatures (<5 K).⁸⁶ The concentration and distribution of F-adatoms on graphene was measured by Raman

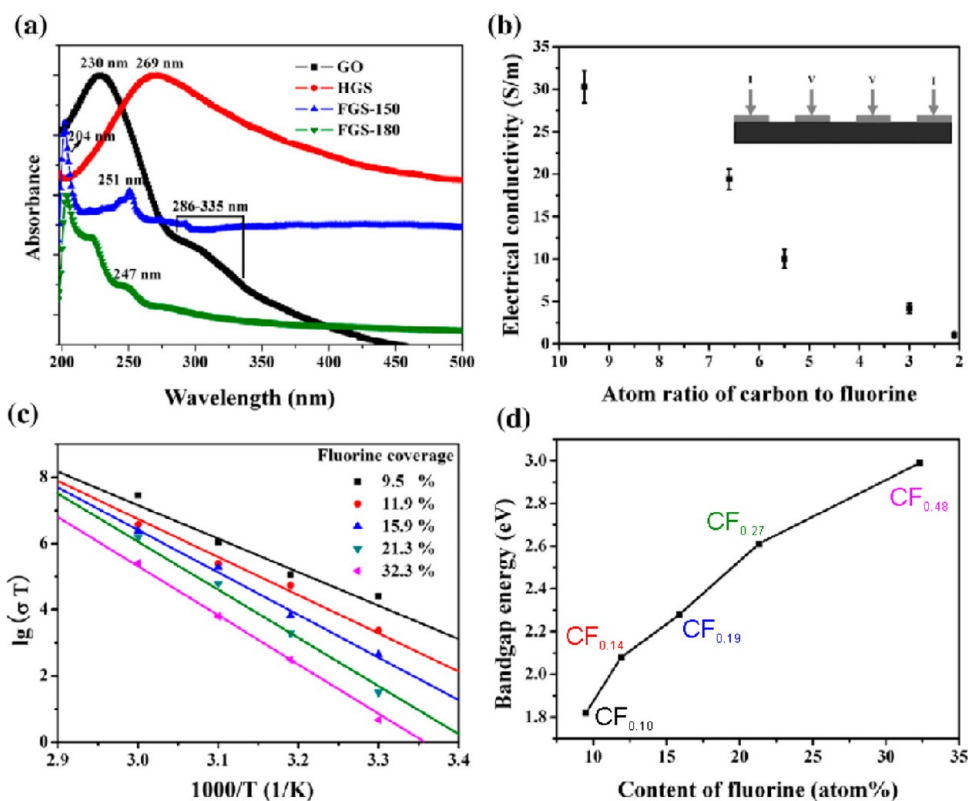


Figure 22. (a) UV–Visible absorption spectra of graphene oxide (GO), hydrothermally reduced graphene sheets (HGS), and two typical fluorinated graphene sheets (FGS) samples (FGS-150 and FGS-180). (b) Electrical conductivities of FGS samples accompanying the variation in C/F ratio. The inset shows a schematic model of the four-probe instrument used. (c) Arrhenius plot for the logarithm of conductivities of fluorinated graphenes series versus the inverse of temperature. (d) Experimental band gap energies of fluorinated graphene (obtained from slopes of lines in panel c subplot) for several F coverages. Reprinted with permission from ref 21. Copyright 2012 Elsevier.

spectroscopy and scanning tunneling microscopy (STM). The resistance at the charge neutrality point increased by 3 orders of magnitude from $25\text{ k}\Omega$ at 200 K to $2.5\text{ M}\Omega$ at 5 K , displaying a strong insulating behavior at dilute F concentration.⁸⁶ Moreover, the presence of adatom-induced local magnetic moments has been reported in dilute fluorinated graphene due to observed spin-flip scattering.⁸⁷ The spin-flip rate was tunable via fluorine coverage and carrier density. Modification of graphene with fluorine may offer a platform for studying magnetism in this unusual two-dimensional electron gas and a gate-controllable, lithography-compatible, approach to control spins in graphene spintronics devices.

Diluted F atoms chemisorbed on graphene have also been investigated theoretically.⁸⁸ It was shown that the nature of the chemical bonding of an F atom adsorbed on top of a C atom in graphene strongly depends on carrier doping. In neutral samples, the F impurities make a sp^3 -like bonding of the C atom below, generating a local deformation of the hexagonal lattice. As the graphene is electron-doped, the C atom withdraws back to the graphene plane and for high doping its electronic structure corresponds to a nearly pure sp^2 configuration. This sp^3 – sp^2 doping-induced crossover provides a new facility for controlling graphene's electronic properties.

Fluorination of graphene has been shown to result in the development of strong paramagnetism with increasing fluorine coverages, that is, in CF_x samples with x increasing from 0.1 to 1 (fluorographene), as well as more than an order of magnitude increase in low- T saturation magnetization (Figure 23a).⁸⁹ For the stoichiometric fluorographene C_1F_1 , a significant decrease in the magnetization was observed compared to $CF_{0.75}$ or $CF_{0.9}$, even though the material showed strong paramagnetism. The number of spins N increased monotonically with x up to $x \approx 0.9$, then decreased slightly for the fully fluorinated samples (Figure 23b). A plot of the number of Bohr magnetons, μ_B , per attached F atom (inset in Figure 23b) clearly showed that the initial increase (up to $x \approx 0.5$) in the number of paramagnetic centers was proportional to x , but a more complicated relation between the number of atoms and N applied at higher x .

Recently, a method to obtain ultrathin, uniform, high- κ , and top-gate dielectrics required to realize the full potential of graphene-based device technologies was developed.³⁷ A 15 nm atomic layer deposition (ALS) Al_2O_3 was uniformly deposited on epitaxial graphene functionalized by fluorine atoms. The underlying graphene properties were not degraded, and 6.7% of the surface of epitaxial graphene was converted to

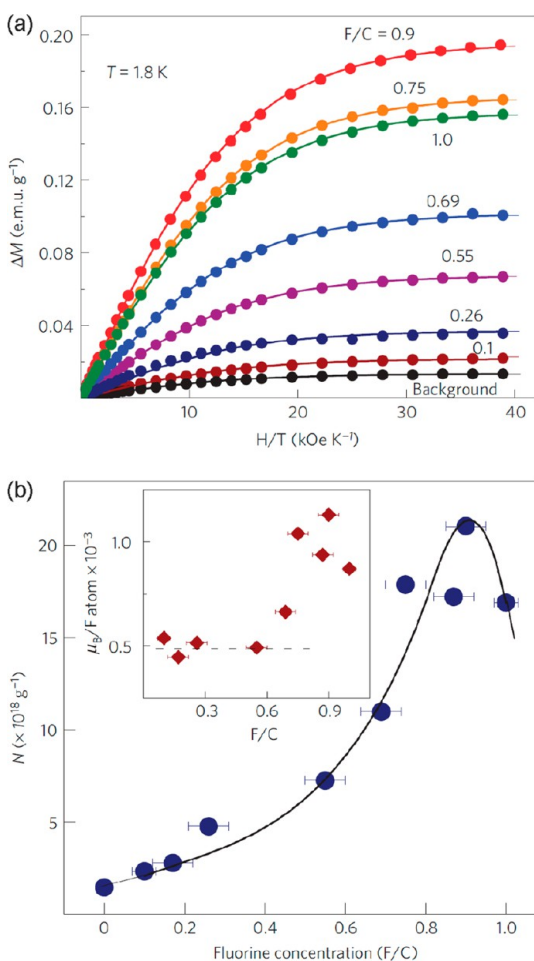


Figure 23. (a) Magnetic moment ΔM (after subtracting linear diamagnetic background) as a function of the parallel field strength H for different F/C ratios. (b) Main panel: number of spins N extracted from the fits in panel a as a function of the F/C ratio. The solid curve is for guidance only. Inset: the same N normalized to the concentration of adatoms in each sample ($\mu_B/\text{F atom}$ is obtained by dividing the number of moments N , assuming that each carries $1 \mu_B$, by the number of F atoms per g of fluorinated graphene). Error bars indicate the accuracy of determination of the fluorine concentrations. Reprinted with permission from ref 89. Copyright 2012 Nature Publishing Group.

C–F bonds which provided enough ALD nucleation sites to obtain conformal films without pinholes.

NEXAFS spectroscopy has been demonstrated to be a powerful technique for evaluating the anisotropy in the chemical bonding of semifluorinated graphite (using a gaseous mixture of BrF_3 and Br_2).⁹⁰ The CK edge NEXAFS spectra of fluorinated HOPG measured at incidence angles of 20° and 90° are compared in Figure 24. This figure shows that the π -system of C_2F is retained after fluorination, as seen from the intense peak near 285 eV. The peak B at 288.5 eV with a shoulder C around 290 eV is related to $1s \rightarrow \sigma^*$ transitions within carbon atoms bonded with fluorine. All three peaks are significantly reduced in intensity when the spectra are recorded at normal incidence (Figure 24d), implying that these peaks (A, B, and C) are

largely due to carbon electrons from orbitals perpendicular to the basal plane. The intensity of D' and D are independent of the beam direction and are associated with transitions involving states of carbon atoms (σ^* states) that are nonbonded or bonded with fluorine atoms. The strong dependence of the intensity of peaks F and G (measured by FK edge spectra) on the incidence of X-ray radiation (Figure 24e and Figure 24f) shows that the C–F bonds have a predominantly perpendicular orientation to the basal plane. This spectroscopic technique helps to shed light on the anisotropic structure of semifluorinated graphite, in which half the carbon atoms are covalently bonded with fluorine, while the rest of the carbon atoms preserve π electrons.

The thermal conductivity of fluorinated graphene has also been studied theoretically by classical nonequilibrium molecular dynamics.⁹¹ The thermal conductivity was found to depend strongly on the coverage and distribution of fluorine atoms. For random fluorination, the thermal conductivity decreased rapidly with increasing fluorine coverage from 0 to 20%, stabilized between 20 and 70%, and then increased rapidly as the coverage approached 100%. The thermal conductivity of graphene fluoride was much less sensitive to tensile strain than that of pristine graphene.

Monte Carlo calculations have suggested that fluorographenes reduce the binding energies of adsorbates (such as $\text{CH}_4, \text{CO}_2, \text{N}_2, \text{O}_2, \text{H}_2\text{S}, \text{SO}_2$) with respect to pure graphene.⁹² In most cases, the adsorption selectivity was greatest for unmodified graphene surfaces and was reduced by fluorination.⁹²

The surface chemistry associated with CF_4^- and Cl_2 -based inductively coupled plasma–reactive ion etching (ICP–RIE) of the 6H-SiC (0001) surface followed by thermal annealing at 970°C has the potential to yield large area graphene-on-insulator films.⁹³

On the basis of the partially fluorinated graphene with composition $\text{CF}_{0.25}$, a novel class of “acceptor type” fluoride intercalated graphite compounds has been proposed.⁹⁴ According to theoretical predictions and experimental evidence, these types of compounds exhibit significantly higher isosteric heats of adsorption for H_2 than previously demonstrated for commonly available, porous carbon-based materials. The unusually strong interaction with H_2 arises from the semi-ionic nature of the C–F bonds. Although high H_2 storage capacity (>4 wt %) at near-ambient temperatures may not be feasible due to diminished heats of adsorption at very high H_2 densities, enhanced storage properties can be envisaged by doping the graphitic host with appropriate species (e.g., nitrogen) to promote more extensive charge transfer from graphene to F^- anions.

Multilayered Fluorinated Graphenes (C_aF_b , $a < b$). Yan *et al.*²² have shown that fluorine-doped multilayered graphene (10 wt %, ~6.6 atom %, synthesized by arc discharge process) sheets exhibit superhydrophobic properties ($\text{CA} \geq 150^\circ$) comparable to that of graphene

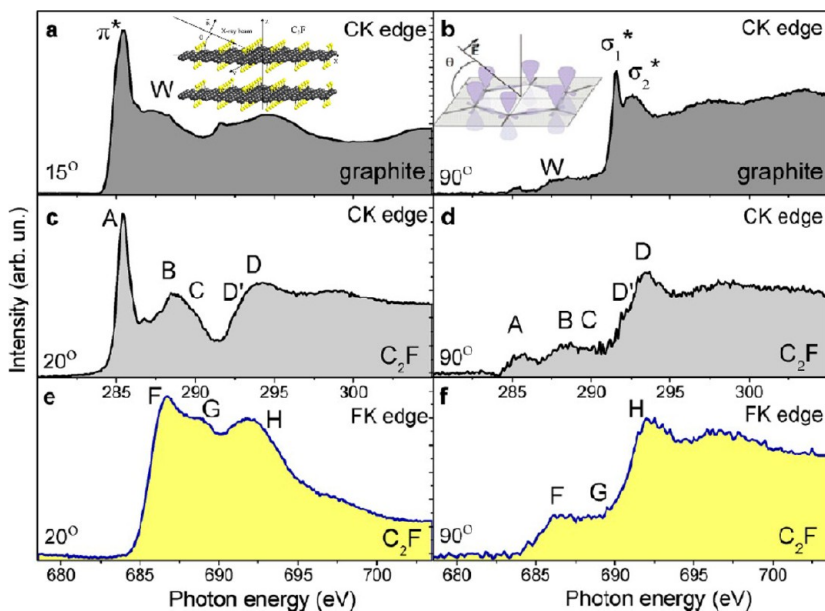


Figure 24. NEXAFS spectra measured near the CK edge of HOPG at an incidence angle θ of radiation of 15° (a) and 90° (b). The inset shows the orientation of the electric field vector of synchrotron radiation relative to the basal plane of graphite. NEXAFS spectra of the fluorinated HOPG measured near the CK edge at grazing (c) and normal (d) incidence, and near the FK edge at grazing (e) and normal (f) incidence. Reprinted from ref 90. Copyright 2012 American Chemical Society.

sheets. The sliding angle of an F-doped graphene sheet film was about 13° compared to about 38° for a pure GS film, indicating that rolling of the droplet on the F-doped GS film was easier than on pure graphene. In addition, the fluorine content in the graphene matrix can be tuned by chemical reaction of graphene oxide with hydrofluoric acid.²¹

Lee *et al.*⁴² have prepared multilayer semi-ionically fluorinated graphene with high insulating properties, which upon reduction with acetone showed a 10^9 times increase in current from 10^{-13} to 10^{-4} A, indicating a transition from insulator- to graphene-like behavior (Figure 25a). The current increase of the reduced fluorinated graphene was much higher with respect to reduced graphene oxide (GO). The reduced multilayered C_2F film showed p-type doped electrical characteristics (Figure 25b). The reduction in acetone proceeds as $2C_2F_{(\text{semi-ionic})} + CH_3C(O)CH_2(l) \rightarrow HF + 2C_{(s)} + C_2F_{(\text{covalent})} + CH_3C(O)CH_2(l)$ at low temperatures. The reduction of multilayered semi-ionically fluorinated graphene film using acetone is well proven by Raman, XPS, and transport measurement analysis (Figure 25c,d).⁴² It should be noted that the XeF_2 treatment is an effective way for high quality fluorination of suspended graphene. However, it is insufficient for multilayered and even bilayered fluorographene.¹² The synthesis proposed by Lee *et al.*⁴² provided several grams of multilayer semi-ionically fluorinated graphene *via* a single step fluorination process for 5 h, which not only generates highly insulating fluorinated graphene (Figure 25a) but could also be used to mass produce fluorinated graphenes for industrial applications. The wetting characteristics of GO changes upon

fluorination due to the low surface free energy of the C–F bonds.⁹⁵ The extent of oxygen coverage on graphene fluoride can be controlled by different reaction conditions to oxidize fluorinated graphite. The material with high fluorine content (23 atom %) in GO was used to create amphiphobic inks for coating on steel, porous substrates.

Bilayer fluorographene C_2F (Figure 26) has been found to be a much more stable material than bilayer graphene.⁹⁶ This is evident by comparison of the formation energies of the final structures and is accentuated by the fact that the formation energy of partially fluorinated bilayer graphane is always negative, in contrast to partially hydrogenated bilayer graphene. The creation of interlayer chemical bonds occurs at higher amounts of fluorination compared with hydrogenation. The electronic band structure of C_2F has been shown to be similar to that of monolayer fluorographene, but its band gap is significantly larger (about 1 eV).⁹⁶ Furthermore, it has been found that bilayer fluorographene is almost as strong as graphene, as its 2D Young's modulus is approximately 300 N m^{-1} .⁹⁶ Structural stability and electronic and magnetic properties of fluorinated bilayer graphene were studied also for various fluorine coverages.^{96,97} Infrared spectral signatures of bilayered surface-fluorinated graphene have been studied by molecular dynamics.^{98,99}

Density functional theory (DFT) computations have revealed the existence of considerable C–H···F–C bonding between graphane and a fluorinated graphene bilayer with a small energy gap (of 0.5 eV at PBE GGA level), much lower than those of individual

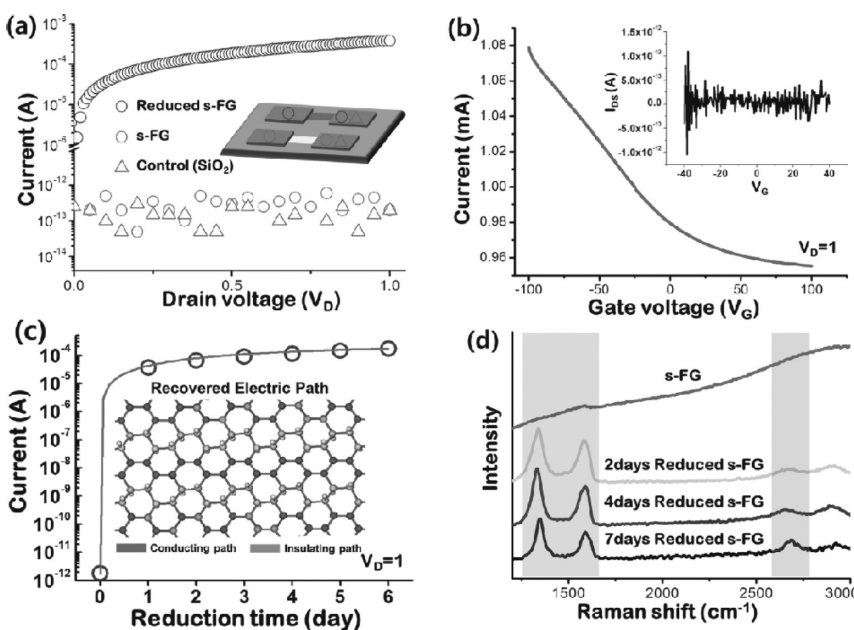


Figure 25. (a) I – V characteristics of multilayered semi-ionically fluorinated graphene films before and after reduction. (b) I – V_g characteristics of a corresponding FET device before (inset) and after the reduction process. (c) Plot showing variation of current on the reduction time. (d) Raman spectroscopy results according to the reduction time. Reprinted with permission from ref 42. Copyright 2013 Wiley.

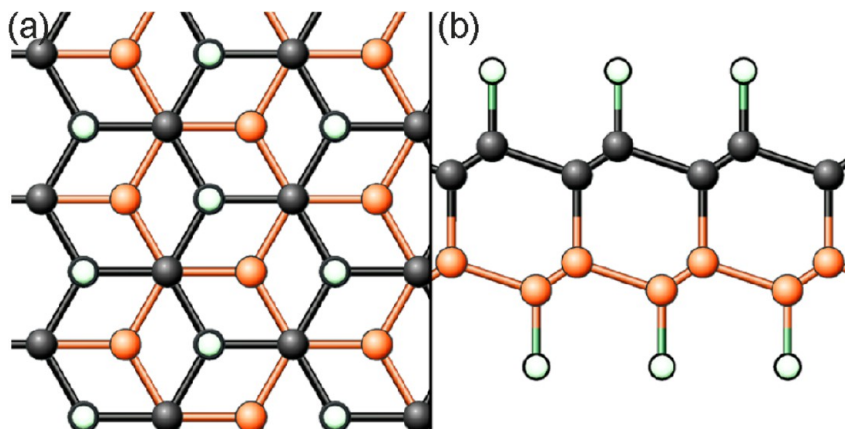


Figure 26. (a) Top and (b) side views of bilayer fluorographene. The carbon atoms in the two layers are shown in different colors for clarity, and the fluorine atoms are indicated by light green (open circles with the smallest diameter). Reprinted from ref 96. Copyright 2012 American Chemical Society.

graphane and fluorographene. The binding strength of this bilayer can be significantly enhanced by an appropriate external electrical field. Changing the direction and strength of the electric field can effectively modulate the energy gap of the G/CF bilayer (0–3.0 eV) and correspondingly causes a semiconductor–metal transition.¹⁰⁰ In sharp contrast, the electronic properties of separated graphane or fluorographene monolayer are rather robust in response to an electric field with corresponding negligible modulation of the band structures.

Halogenated Graphenes (C_aX_b , $X = \text{Cl}, \text{Br}, \text{I}; a \leq b$). **Chlorographene.** The fully chlorinated graphene (chlorographene, graphene chloride, or CCl) has been broadly theoretically discussed,^{13,56–59,75} but not yet

prepared. The pristine parent material, graphite chloride, is unstable at temperatures >0 °C, but stable at lower temperatures;¹⁵ therefore it is reasonable to assume that CCl is unstable under ambient conditions. On the other hand, its instability has not yet been proven experimentally. Moreover, partially chlorinated graphene derivatives have been reported recently.^{25–28} However, the coverage of chlorine atoms was maximally up to 30 atom % ($\text{CCl}_{0.43}$). The stability of such compounds has been confirmed from room temperatures to 500 °C.²⁸ Therefore, the existence of chlorographene is still uncertain and further experiments are needed to verify whether CCl is stable at room temperature.

The lattice constant and C–C distance in the chair conformation of chlorographene (2.91 Å and 1.76 Å)

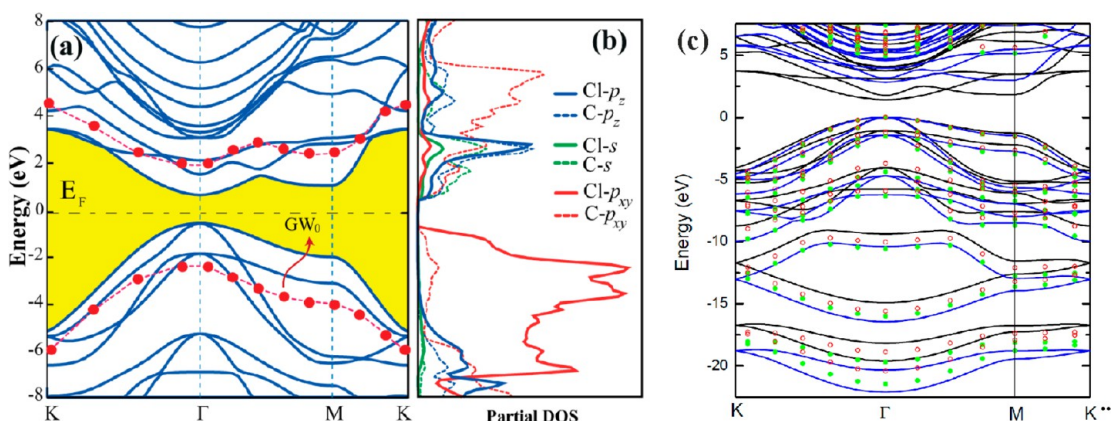


Figure 27. (a) Electronic band structure of chlorographene CCl. The LDA band gap is shaded yellow. The GW_0 corrected valence and conduction bands are shown by a dashed line and red balls. The zero of energy is set to the Fermi level, E_F . (b) Density of states projected to various orbitals (PDOS). Reprinted from ref 75. Copyright 2012 American Chemical Society. (c) Comparison of CCI band structures calculated using the PBE functional (black line), HSE06 functional (blue line), GW over PBE (red circles), and GW over HSE06 (green dots). The Fermi level was set at zero energy. Reprinted from ref 59. Copyright 2013 American Chemical Society.

have been predicted at the GGA DFT level to be notably larger than the equivalent parameters for fluorographene (2.61 Å and 1.58 Å) and graphane (2.54 Å and 1.54 Å),^{57–59} and the C–C distance is significantly deviated from typical values for a single C(sp³)–C(sp³) bond (~1.54 Å). This is because chlorine atoms attached to the perturbed graphene sp³ lattice partially overlap with each other and the whole lattice must balance C–C bonding with Cl–Cl repulsion.⁵⁸ Consequently, CCl is less stable than CH and CF.

Surprisingly, initial theoretical calculations of the electronic structure of CCl (ref 56) suggested metallic behavior. This was probably due to “nonbonded” structures (composed of carbon sp² net and adsorbed chlorine atoms) reported later⁵⁷ and confirmed recently by consideration of the reaction mechanisms of Cl atoms and graphene¹⁰¹ or Cl atom adsorption.^{26,102} The reported chlorographene GGA DFT band gap of 1.4 eV^{57–59} corresponding to an sp³ “bonded” chair structure indicates semiconducting or insulating properties. However, the GGA band gap values may be seriously underestimated. More realistic is the value of 2.8 eV^{58,59} obtained using the hybrid (HSE06) functional. The bottom of the conduction-band and top of the valence-band are located at the Γ point in the first Brillouin zone, the top of the valence band is doubly degenerate, and the maximum band gap is located at the K point (Figure 27). Similar to fluorographene, the high-level many-body GW approximation which includes electron–electron interactions beyond DFT, predicted a dramatically increased band gap of 4.3–5.2 eV (depending on the GW level and orbitals used).^{59,75}

It has been reported⁷⁵ that all the phonon modes of chairlike CCl have positive frequencies (Figure 28a), and hence the predicted structure of chlorographene is stable at $T = 0$ K. Although chlorographene belongs to the same space group, D_{3d} , as CH and CF, the

phonon frequencies are lowered (softened) due to saturation of the C atoms with heavy Cl atoms (*cf.* Figure 28a versus Figure 14a for CF). Group theory analysis has shown that the decomposition of the vibration representation at the Γ -point is $\Gamma = 2A_{1g} + 2A_{2u} + 4E_g + 4E_u$. Among these, the modes at 105, 398, 751, and 1042 cm⁻¹ (Figure 28a) are bond stretching modes and are Raman-active. The Raman mode A_{1g} at 1042 (398) is entirely due to the out-of-plane vibration of C and Cl atoms moving in the same (opposite) direction with respect to each other (*cf.* Figure 14b). Further observation of these Raman active modes is expected to shed light on the Cl coverage and the structure of chlorinated graphene.

Comparison of the optical absorption spectrum of CCl obtained at the DFT+RPA and G_0W_0 +RPA levels shows (Figure 28b) that inclusion of electron–electron interaction leads to blue shift of the absorption due to quasi-particle corrections; however, spectra shape is preserved.⁵⁹ On the other hand, the inclusion of the electron–hole correlations yields a significant red shift of the absorption spectrum (insets in Figure 28b) similar to fluorographene (Figure 13). A prominent physical effect of the electron–hole interactions is apparent for some bound excitons below the G_0W_0 gap (see insets in Figure 28b), which are completely missing in the G_0W_0 +RPA. The first exciton peak of the CCl spectra is located at 2.82 eV with a corresponding binding energy of 1.25 eV.⁵⁹

Properties of Chlorinated Graphenes. Adsorption of the Cl atom on graphene has been mainly studied theoretically.^{26,75,101,102} The adsorption of a single Cl atom was shown to be significantly different from that of H and F. A charge-transfer complex (where C orbitals maintain a planar sp² net) was predicted. The C–Cl distance was notably larger than that of CF and CH (covalent bond), suggesting that the carbon net is not

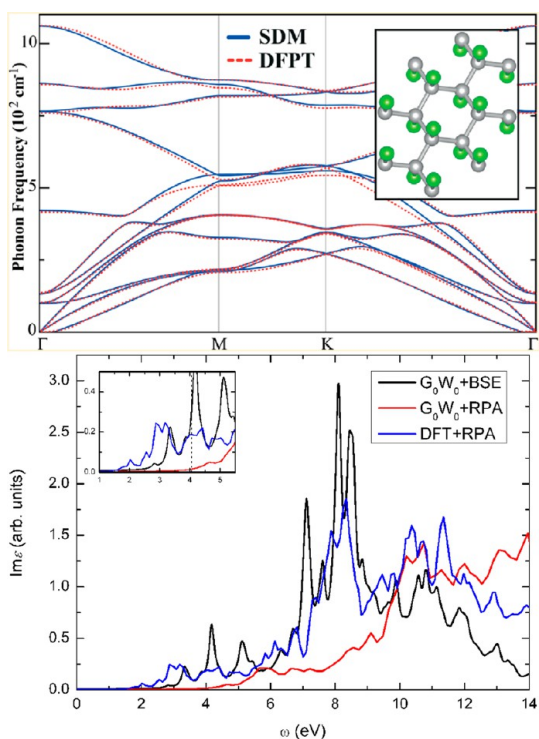


Figure 28. (a) Phonon bands of chlorographene calculated using the SDM (small displacement method) and DFPT (density functional perturbation theory) methods. Inset: structure of chair CCl. Reprinted from ref 75. Copyright 2012 American Chemical Society. (b) Absorption spectra of chlorographene for light polarization parallel to the surface plane. The insets contain amplified absorption spectra in the vicinity of the first exciton peak and G_0W_0 (PBE) gap (dashed line). Reprinted from ref 59. Copyright 2013 American Chemical Society.

as buckled (Figure 29).¹⁰¹ Various adsorption configurations were possible during the adsorption of other chlorine molecules (Figure 30). However, not all possible configurations or patterns obtained by the chlorination of one surface of graphene were stable.⁷⁵ When both sides of the graphene sheet were exposed, the Cl atoms preferred to form homogeneous patterns, and the optimal coverage was 25%, in contrast to the value of 100% in hydrogenation and fluorination.¹⁰¹ Interestingly, DFT calculations have shown that chlorine binds to the graphene edges more easily than adsorbing on the graphene plane and graphene could be broken into edges by chlorine.¹⁰² Those results could serve as an alternative explanation of the photochemical chlorination experiment.²⁵

The presence of the characteristic D-peak at 1330 cm^{-1} , the G-peak at 1587 cm^{-1} , and the 2D-peak at 2654 cm^{-1} (Figure 31a; cf. 1580 and 2680 cm^{-1} for graphene) from chlorinated graphene indicates a low coverage of Cl (expected ~ 8 atom %).²⁵ For higher coverage (~ 21 atom %), the obvious D peak located at 1359 cm^{-1} in the Raman spectrum of $\text{CCl}_{0.21}$ (Figure 31b) indicates that during the chlorination process, larger quantities of covalent C–Cl bonds were formed in graphene sheets, and thus a high degree of

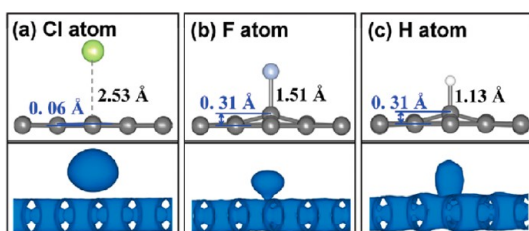


Figure 29. Adsorption of a single (a) Cl, (b) F, or (c) H atom on graphene from LDA. Structures with partial parameters are shown in the upper panels, and electron localization function (ELF) plots with an isosurface value of 0.70 are depicted in the bottom panels. Reprinted from ref 101. Copyright 2012 American Chemical Society.

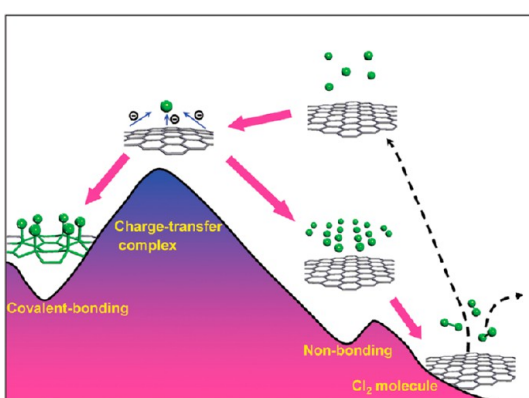


Figure 30. Schematic representation of how various adsorption configurations evolve during chlorination of graphene. Reprinted from ref 101. Copyright 2012 American Chemical Society.

crystalline disorder was generated by the transformation from sp^2 to sp^3 configuration.²⁷ The covalent attachment of Cl atoms on the graphene sheets (C–Cl bonding) has been confirmed by XPS and IR spectroscopic analysis. Since the Raman measurements were performed in the range from 1000 or 1250 cm^{-1} to higher frequencies, possible low-frequency Raman-active peaks originating from chlorine atoms could not be observed (vibrational modes up to 1050 cm^{-1} are theoretically predicted for CCl (Figure 28)). However, lower frequencies were recorded in the infrared spectra of chlorinated samples (Figure 31c). A band at 790 cm^{-1} (930 cm^{-1}) was reported for ~ 30 atom %²⁸ (~ 5.9 wt %⁴⁸) coverage of chlorine atoms, which was assigned to the C–Cl stretching vibration.²⁸ Only one vibrational mode was suggested by theoretical calculations of CCl which may correspond to this band: the A_{2u} mode at $\sim 850 \text{ cm}^{-1}$, which is infrared active (Figure 28).⁷⁵

The chlorinated graphene samples were shown to be stable under ambient conditions, and therefore can be stored for long periods. The thermal stability of $\text{CCl}_{0.43}$ was examined in detail by IR and energy dispersive X-ray analysis (EDAX) spectra.²⁸ A decrease in the C–Cl band intensity was observed upon heating progressively, and it completely disappeared above 500°C (Figure 31c).

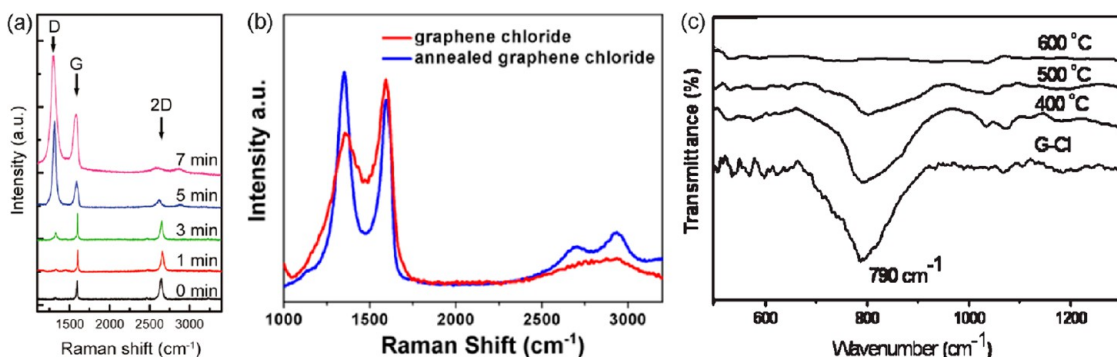


Figure 31. (a) Raman spectra (wavelength $\lambda_{\text{ex}} = 632.8 \text{ nm}$) evolution with time for single-layer graphene reacted with chlorine under xenon lamp irradiation. Reprinted from ref 25. Copyright 2011 American Chemical Society. (b) Raman spectra of chlorinated graphene prepared by microwave-spark (MiW-S) assisted reaction. Reprinted with permission from ref 27. Copyright 2012 Nature Publishing Group. (c) IR spectra of CCl_x heated for 4 h at various temperatures. Reprinted with permission from ref 28. Copyright 2012 Royal Society of Chemistry.

The Cl coverage can be used to tune the graphene band gap. Typically, the partially chlorinated graphene exhibited a nonzero band gap and displayed a 4 orders of magnitude higher sheet resistance than graphene (8% coverage of chlorine atoms).²⁵ The higher resistance can be explained by perturbation of the graphene π -conjugated systems upon the chlorination process. Furthermore, the dielectric constant (ϵ) of the chlorinated reduced graphene oxide composite film ($\epsilon = 169$) was found to be much higher than untreated reduced graphene oxide composite film ($\epsilon = 24$).¹⁰³ The large enrichment in the dielectric constant is attributed to the interfacial polarization between the chlorinated reduced graphene oxide platelets and the polymer, along with the polar and polarizable C–Cl bonds. These chlorinated reduced graphene oxide platelets also displayed a 93% increase in conductivity, due to p-type doping effect created by Cl atoms.

Properties of Brominated Graphenes. Fully brominated graphene (graphene bromide) is unstable, and metallic behavior is predicted from calculations (Figure 32).^{56–58} The predicted lattice constant, C–C, and C–Br distances are 3.11, 1.86, and 1.92 Å, respectively, at the GGA DFT level.⁵⁷ However, preparations of a few-layer graphene brominated up to 4.8 atom % by UV irradiation in liquid-bromine medium²⁸ and graphene brominated up to 4 atom % using microwave-spark assisted reaction²⁷ have been reported. The D peak (~1350 cm⁻¹) of brominated graphene (Figure 33a) has been shown to be weaker than that of chlorinated graphene, possibly due to the lower degree of modification. Compared with the band for pristine graphene, the strong and symmetric 2D peak of $\text{CBr}_{0.04}$ was blue-shifted (8 cm⁻¹) and became broader, consistent with the small extent of modification by Br.²⁷ The infrared spectrum of the brominated graphene (9.9 wt %, 1.6 atom %) obtained from thermally reduced graphene oxide (TRGO) showed a vibration at 600 cm⁻¹ (Figure 33b), which is indicative of a C–Br bond in TRGO-Br.⁴⁸

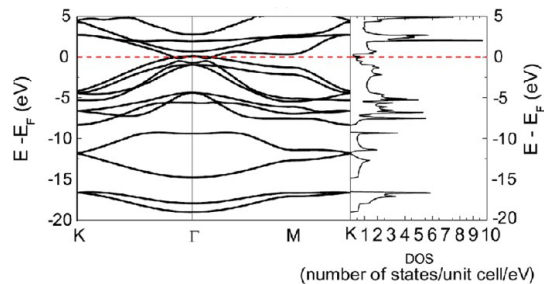


Figure 32. Graphene bromide: band structure along the directions joining some high symmetry points of the Brillouin zone and density of states. Reprinted with permission from ref 57. Copyright 2010 Institute of Physics.

Changes in the electronic properties of few-layer graphenes doped by adsorption and intercalation of Br_2 vapors have been studied by Raman spectroscopy.¹⁰⁴ The π conjugation network of graphene remained unaffected after halogen doping. Adsorption of bromine on single-layer graphene created a high doped hole density, well beyond that achieved by electrical gating with an ionic polymer electrolyte. In addition, the 2D Raman band was completely quenched. The bilayer spectra indicated that doping by adsorbed Br_2 was symmetrical on the top and bottom layers. Br_2 intercalated into 3-layer and 4-layer graphenes. The combination of both surface and interior doping with Br_2 in three and four layers created a relatively constant doping level per layer. For graphene with three or more layers, a resonant Raman signal was observed for Br_2 at around 238 cm⁻¹; for monolayer and bilayer graphene, no bromine signal was observed (Figure 33c).¹⁰⁴ This could be an orientation effect, since, if the Br_2 sits perpendicular to the surface as LDA DFT calculations suggest¹⁰⁵ and orthogonal Raman is used, the molecules would be aligned with the beam and there would be no interaction, and hence no signal. It has been shown that the halogen molecule forms a $\text{Br}^+ + \text{Br}^-$ pair, rendering it infrared active, and has an empty p_z orbital located in the graphene electronic π cloud.¹⁰⁵

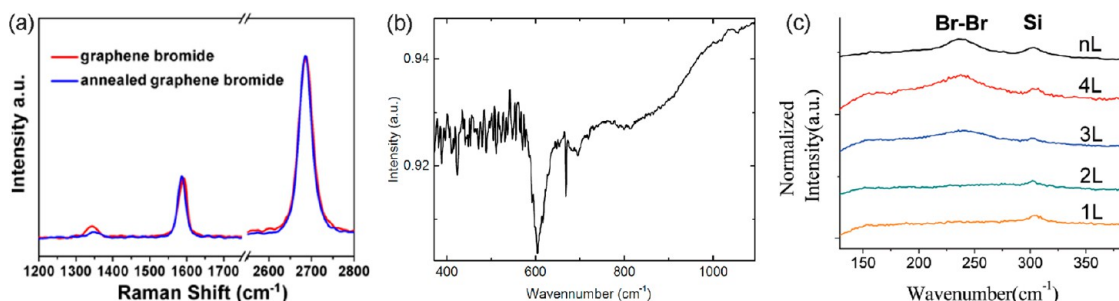


Figure 33. (a) Raman spectra of brominated graphene prepared by microwave-spark (MiW-S)-assisted reaction. Reprinted with permission from ref 27. Copyright 2012 Nature Publishing Group. (b) FTIR spectra of brominated graphene showing C–Br peak at 600 cm^{−1}. Reprinted with permission from ref 48. Copyright 2013 Wiley. (c) Br₂ stretching region of Raman spectra for few-layer (L) graphenes exposed to bromine. The weak 303 cm^{−1} peak labeled Si is due to the underlying crystalline silicon substrate. The Br–Br peak near 240 cm^{−1} is due to intercalated bromine (see also scheme of Figure 34c). Reprinted from ref 104. Copyright 2009 American Chemical Society.

Bromination opens a small band gap (\sim 86 meV at LDA level) and strongly dopes the graphene. The described molecule was identified as a new form of Br₂ previously only considered as an unstable intermediate of bromine-induced carbon-bond saturation.¹⁰⁵

Iodine-Doped Graphene. Iodine-doped graphenes can be prepared by direct heating of camphor and I₂ with an iodine loading of 3 atom %.⁴⁶ In addition, exfoliation of graphene oxide and I₂ under ultrasonic treatment followed by thermal annealing at various temperatures (500–1100 °C) generates iodine-doped graphenes (1.2–0.8 wt %; \sim 0.1 atom %).⁴⁷ These samples showed good electrocatalytic activity and methanol tolerance for the oxygen reduction reaction.⁴⁷ X-ray photoelectron and Raman spectroscopic analyses have confirmed the presence of elemental iodine in the form of triiodide (I₃[−], peak at 117 cm^{−1}) and pentaiodide (I₅[−], peak at 154 cm^{−1}) in these doped samples (Figure 34a),^{46,47} which is not surprising as iodographene (fully iodinated graphene, graphene iodide, Cl) has been identified as an unstable and spontaneously decomposing compound.¹³ It is worth noting that iodographene was identified as a metastable intermediate in the exchange reaction of eq 1 in DMF as the solvent (in sulfolane, the considerably faster kinetics pass). The reaction occurs at just 150 °C and the IR peak corresponding to the C–I unit (745 cm^{−1}) was observed.¹³

Iodine doped graphene obtained from TRGO has been shown to exhibit two additional peaks at approximately 90 and 167 cm^{−1} that are absent in the Raman spectra of TRGO-Cl and TRGO-Br.⁴⁸ The peak at 90 cm^{−1} was attributed to the presence of I₃[−] in the material, whereas the presence of I₅[−] gave rise to the peak at 167 cm^{−1}. The emergence of these peaks indicates the successful incorporation of iodine atoms into the TRGO during the exfoliation procedure.

Jung and co-workers¹⁰⁴ have studied changes in the electronic properties of few-layer graphenes doped by adsorption and intercalation of I₂ vapors by Raman spectroscopy. The π conjugation network of graphene

remained unaffected after the halogen doping. In contrast to Br₂ (see above), the Raman G peak of three or four layers with surface adsorbed I₂ indicated that the hole doping density was larger on the surface layers than on the interior layers and that I₂ does not intercalate into three or four layers. This adsorption-induced difference between surface and interior layers implied that a band gap opens in the bilayer-type bands of three or four layers (Figure 34b). A comparison of possible graphene doping by adsorption and intercalation of I₂ with respect to Br₂ is shown in the schematic diagram of Figure 34c.¹⁰⁴

The interaction of various halogen molecules, such as ICl, Br₂, IBr, and I₂, with few-layer graphene has been studied by Ghosh *et al.*¹⁰⁶ Halogen molecules, being electron withdrawing in nature, induce distinct changes in the electronic states of graphene, as evident by changes in the Raman and electronic absorption spectroscopy. The magnitude of the molecular charge-transfer between the halogens and the graphenes varied in the order ICl > Br₂ > IBr > I₂.

Mixed Graphene Halides and Hybrids. In early calculations on hydrogenated and halogenated graphenes, hypothetical mixed structures C₂H_X (X = F, Cl, Br, I) were also tested.^{56,57,107} Structures with H and X on different sides of graphene were predicted to have a nonzero band gap in the case of X = F, Cl (3.1 eV for C₂HF and 0.8 eV for C₂HCl at GGA DFT level or 6.4 and 2.9 eV at G₀W₀ level, respectively),⁵⁶ whereas metallic behavior was predicted for heavier halogens (C₂HBr and C₂HI). Hybrid compounds C₂LiF and C₂LiH were reported as weak metal and semimetal, respectively. Very recently, a piezoelectric effect was predicted for six conformations of different-side C₂HF and C₄HF compounds.¹⁰⁸

Recently, hypothetic homogeneous-side mixed halides have been suggested.⁵⁸ All of the optimized C_aX_bY_c (X = H, F; Y = F, Cl, Br, I for Y ≠ X) compounds were considered and shown to be direct band gap materials. The results showed that the bottom of the conduction band and top of the valence band are located at the Γ point in the first Brillouin zone for

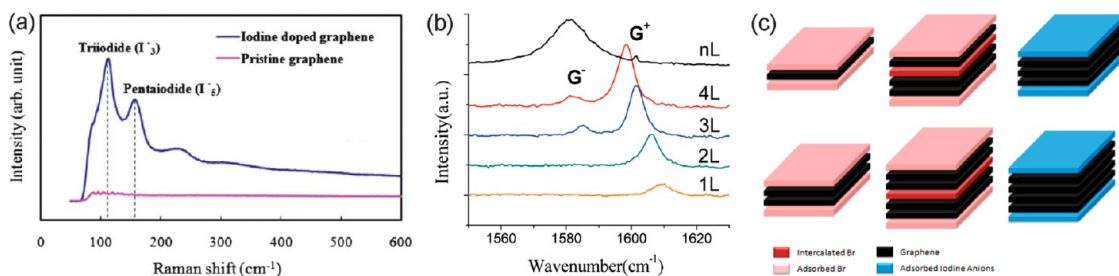


Figure 34. (a) Raman spectra at low wave numbers showing formation of triiodide and pentaiodide in the graphene structure. Reprinted with permission from ref 46. Copyright 2011 Royal Society of Chemistry. (b) G peak Raman spectra of few-layer graphenes and graphite exposed to iodine vapor. The curves are vertically displaced. The relative intensity change from 1 layer to graphite is shown. The G-peak of doped few-layer graphene samples is smaller than that of the 1580 cm^{-1} undoped graphite G peak, as expected for doped samples. In graphite, a small peak at 1601 cm^{-1} may correspond to surface graphene layers with adsorbed I_2 . (c) Schematic diagram of few-layer graphenes exposed to Br_2 (left) and I_2 (right). On the left side, the 3-layer and 4-layer structures have both intercalated (dark pink) and adsorbed (light pink) Br_2 layers. On the right side, the three-layer and four-layer structures have surface adsorbed (light blue) iodine anion layers without intercalation. Reprinted from ref 104. Copyright 2009 American Chemical Society.

all $C_aX_bY_c$ species. The top of the valence band is doubly degenerate and the maximum band gaps are located at the K points in CH, CF, CCl, and CBr. The band gap depends on the stoichiometry (chemical composition) and can be relatively smoothly tuned from the maximal value in graphane to almost zero in graphene bromide (Figure 35a). Even finer tuning could in principle be achieved by adjusting the ratio of more than two substituents. Most of the considered species appeared to have band gaps typical of insulators. Two species had band gaps comparable to those of conventional semiconductors. Specifically, the band gaps of C_2FBr and C_2HBr were 1.32 and 1.55 eV (at HSE06 level), respectively. However, the latter is probably unstable.

Stability of Halogenated Graphenes. The stability of graphene derivatives is usually assessed by considering quantities such as the binding energy, energy of formation, or vibrational modes. All of the considered materials are of similar type and stoichiometry, and therefore it is possible to evaluate their stability through the following exchange reaction (for single supercells):^{13,58}



Here, the product $C_aX_bY_c$ ($a = b + c$; X = H, F; Y = F, Cl, Br, I for $Y \neq X$) is the target material and $\Delta E'$ is the difference between the sums of the total energies of the products and the reactants. To compare the stability of different materials, it is better to consider the normalized energy difference $\Delta E = \Delta E'/(2a)$, where a is the number of C atoms in a computational supercell. The choice of a reference material assigned with zero ΔE (and reactant in eq 2) is rather arbitrary, but a stable and experimentally prepared material is preferred. Of the two such available 2D graphene-based materials, graphane (CH) and fluorographene (CF), the former with lower stability is the better choice since it is possible to obtain a simple indication of the stability from the ΔE value. If a $C_aX_{a-c}Y_c$ compound is more

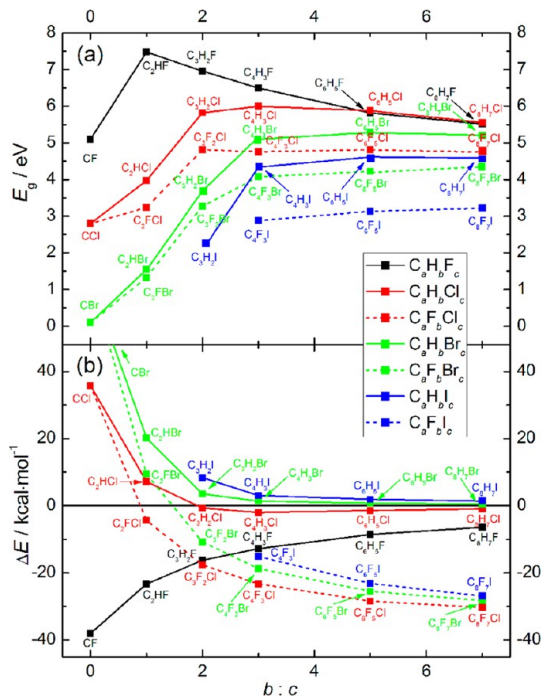


Figure 35. Electronic band gaps (a) and stabilities (b) of graphene derivatives $C_aX_bY_c$ ($a = b + c$) as a function of the stoichiometric ratio $b:c$ for selected substituents X = H, F and Y = F, Cl, Br, I calculated using the HSE06 functional. The limits of $b:c \rightarrow 0$ [∞] correspond to CF, CCl, and CBr [CH and CF]. Reprinted with permission from ref 58. Copyright 2012 American Institute of Physics.

stable than CH, ΔE would be negative. A positive value of ΔE indicates that the species is less stable than CH but not necessarily thermodynamically unstable. Comparison of ΔE values (Figure 35b) shows that the most stable of the graphene halide derivatives is fluorographene. The decrease in stability on going from CF to CCl to CBr and finally to Cl (which spontaneously decomposes to iodine and graphene¹³) is a consequence of the halogen atoms being forced into excessively close proximity by the graphene halide scaffold (Figure 36). The lower bound of stability is considered

to be ΔE for CCl because the pristine parent material, graphite chloride, is unstable at temperatures >0 °C but stable at lower temperatures.¹⁵ On the other hand, nonstoichiometric graphene chloride with lower concentrations of Cl has recently been prepared.^{25–28} Moreover, some samples (few-layer graphene chlorinated up to 30 atom %) have been shown to be stable at room temperature and the chlorine can be removed by heating to around 500 °C or by laser irradiation. Very recently,⁷⁵ theoretical analysis using finite temperature *ab initio* MD calculations have suggested that a perfect CCl is stable at $T=0$ K and can remain stable possibly at room temperature. The creation of a single vacancy at one site imposes the formation of a second vacancy at the opposite side. This pair of vacancies can survive at room temperature. However, the presence of vacancies or holes would make CCl vulnerable to dissociation through the formation of Cl₂ molecules.⁷⁵

Patterned Halogenation. Selective fluorination or chlorination of graphenes is an interesting approach for generating materials with applications in graphene-based electronic devices.^{12,16,20,33} Patterned halogenation of graphene can be achieved using appropriate masks or grids. During this process, only exposed regions are fluorinated or chlorinated, whereas those protected by the mask remain unaltered. These masked regions could be used as conductive pathways in graphene-based devices. Cheng *et al.*¹⁷ have suggested that graphene nanochannels surrounded by insulating fluorographene *via* patterned fluorination could provide an alternative to nanoribbon structures. Lee *et al.*³⁶ have developed a device comprising graphene nanoribbon (GNR) surrounded by fluorinated graphene with a composition of C₄F and shown it has an electron mobility of ~ 2700 cm²/(V·s). First, GNRs as narrow as 35 nm were fabricated by using scanning probe lithography to deposit a polystyrene mask and then fluorinating the sample to isolate the masked graphene from the surrounding wide band gap fluorinated graphene. In this case, the fluorinated regions retained the starting carrier mobility and exhibited stable p-doping of 0.17 eV, while the polymer mask containing GNR also showed stable performance.

The properties of graphene nanorods and hexagonal nanodots inside fluorographene⁶³ and in fluorographene ribbons¹⁰⁹ have been studied theoretically. It has been shown that the orientation (zigzag (ZZ) or armchair (AC)), width of graphene nanorods, and F coverage affects its properties, e.g., band gap (Figure 37). Fluorinated graphene nanoroads with AC orientation are semiconducting with large band gaps, following a nonmonotonic variation. Nanoroads with a ZZ edge are semiconducting or semimetallic according to their spin orientation, that is, antiferromagnetic or ferromagnetic, respectively. The band gaps in ZZ roads vary as $\sim 1/N_{zz}$.⁶³ Thus, graphene nanoroads behave like graphene ribbons. In contrast, the hexagonal and

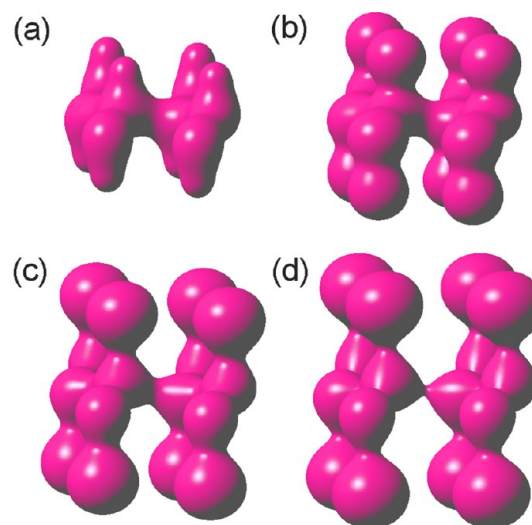


Figure 36. Total electron densities of (a) graphane (CH), (b) fluorographene (CF), (c) graphene chloride (CCl), and (d) graphene bromide (CBr) in a 2×2 supercell for isovalue of 0.1 au. The distances shown correspond to optimized geometries: the C–C distances are (a) 1.53 Å, (b) 1.57 Å, (c) 1.74 Å, and (d) 1.84 Å. Notice the decreasing electron density in the middle of the C–X bond and the C–C bond with increasing size of the halogen atom. Reprinted with permission from ref 58. Copyright 2012 American Institute of Physics.

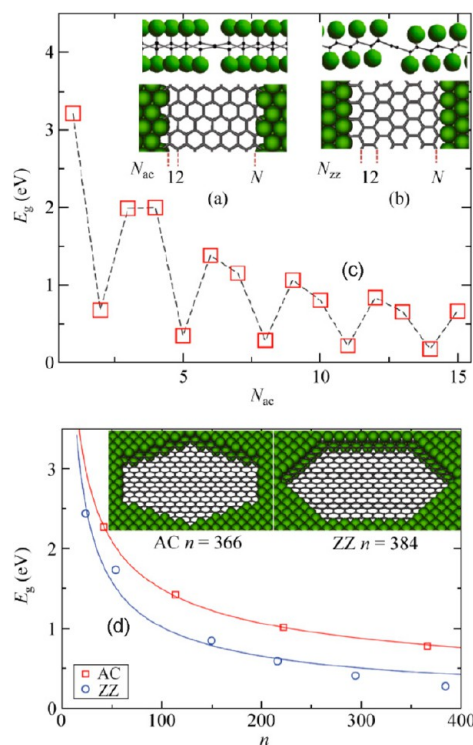


Figure 37. Schematic illustrations of (a) armchair (AC) (N_{ac} is the number of sp² C dimer lines), and (b) zigzag (ZZ) (N_{zz} is the number of sp² C chains) roads. (c) For AC nanoroads, the band gap E_g energy varies with the road width N_{ac} . (d) Plots showing how the energy of the band gap for dots with AC and ZZ edges decreases with their size. Inset: configurations of the largest optimized quantum dots. Reprinted with permission from ref 63. Copyright 2011 Springer.

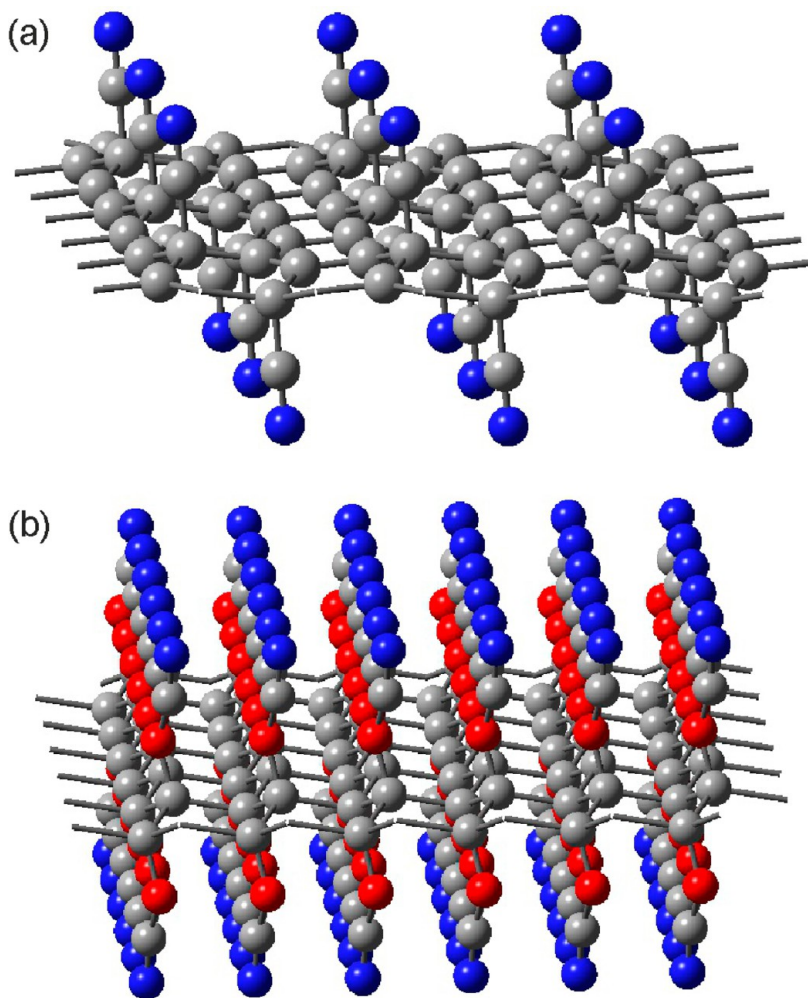


Figure 38. (a) Partially covered graphene derivative $C(CN)_{0.25}$. (b) Fully covered graphene derivative $COCN$.

triangular patterned vacancies in the fluorographene structure have been shown to behave like quantum dots.^{63,110} Nonetheless, the presented properties are not an unique feature for halogenated graphene structures because similar behavior was reported for graphene nanorods¹¹¹ or nanoribbons^{112,113} and hexagonal nanodots inside graphane.¹¹⁴ Graphene nanoribbons with various degree of fluorination up to full fluorination (i.e., rather an inverse system to the previously mentioned graphene nanoroads inside fluorographene, however, with the same interfaces graphene/fluorographene) were also studied. Both fully fluorinated ZZ and AC graphene nanoribbons were predicted to be semiconductors with width-dependent energy gaps.¹¹⁵ ZZ hybrid nanoribbons with an F-terminated edge in the antiferromagnetic state were shown to be half-semiconductors, in which the spin degeneracy near the Fermi level was completely broken. In contrast, hybrid armchair nanoribbons were suggested to be nonmagnetic semiconductors. Interestingly, the results suggested that the electronic properties of partially fluorinated ZZ graphene nanoribbons could be finely tuned by edge chemical

modification and control of the width of fluorinated graphene.¹¹⁵

Later, it was shown that the resistivity of insulating fluorinated graphenes can be progressively decreased by several orders of magnitude simply by electron beam irradiation.¹¹⁶ The electron-irradiated fluorinated graphene ultimately exhibited a similar resistance per square to that of pristine graphene. The decrease in resistivity was attributed to fragmentation of C–F bonds induced by electron irradiation. Results showed that standard electron beam patterning processes can be used to engineer conductive and semiconductive structures with sizes ranging from a few micrometers down to a few tens of nanometers. This opens up new avenues for the fabrication of graphene-based transparent and flexible electronic devices, with defluorinated graphene channels that can be used as metallic interconnects or elements of device structures. Furthermore, patterning channels with different conductivities may lead to the development of novel resistive memory and data storage devices, with multiple byte levels associated with different resistivities.

Conclusion and Future Challenges. This review shows that stoichiometric fluorographene is already, together with graphane and graphene oxide, a well-established member of the family of graphene derivatives with broad application potential. Nevertheless, there are still some discrepancies related to hydrophobicity/hydrophilicity of fluorographene or to its exact band gap value. Despite of a huge progress in research of other partially halogenated and mixed graphene halides, there are many challenges related to the controlled synthesis, properties, and band gap engineering of these structures. No doubt, new straightforward methods for the preparation of various halogenated and mixed halogenated graphenes are likely to be developed in the near future.

One of important challenges include the synthesis and complex analysis of “pseudohalides”, at least C—CN (Figure 38a) and C—OCN (Figure 38b). Similarly, substitution of halogen atoms by suitable functional groups would bring a high additional value for chemical and sensing application; the same situation is expected in the case of functionalization through organometallics, R—Mg—X. Concerning challenges in the field of applications of graphene halides, colloidal fluorographenes are promising materials for the design of novel polymer nanocomposites and protective coatings. Moreover, interesting electronic and transport properties may arise due to stacking of fluorographenes/graphene or graphene/fluorographene/graphene (G/CF/G), which would act as nanocapacitors analogous to G/BN/G. Halogenated and stacked graphenes can also be utilized for storing/adsorption of important gases, for example, hydrogen storage. We envisage a great potential for the halogenated graphenes also in the fields of optics, biology, or electrochemistry. This large scale of applications would be even enlarged in the future also with respect to the expected new kinds of graphene halides. This is, for example, the case of recently developed fluorinated graphene quantum dots (F-GQDs) exhibiting bright blue photoluminescence and a clear upconversion photoluminescence.¹¹⁷ Similarly, Janus-like asymmetric graphenes produced by capping of halogens would find applications as novel sensors, actuators, and surfactants because of their interesting surface properties.¹¹⁸

Conflict of Interest: The authors declare no competing financial interest.

Acknowledgment. The authors acknowledge support by the Operational Program Research and Development for Innovations—European Regional Development Fund (CZ.1.05/2.1.00/03.0058 of the Ministry of Education, Youth and Sports of the Czech Republic), the Operational Program Education for Competitiveness—European Social Fund (CZ.1.07/2.3.00/20.0017 of the Ministry of Education, Youth and Sports of the Czech Republic), and the Czech Science Foundation (P208/12/G016). K.K.R. Datta acknowledges financial support by the Operational Program Education for Competitiveness—European Social Fund (project CZ.1.07/2.3.00/30.0041 of the Ministry of Education, Youth and Sports of the Czech Republic).

REFERENCES AND NOTES

- Novoselov, K. S.; Fal'ko, V. I.; Colombo, L.; Gellert, P. R.; Schwab, M. G.; Kim, K. A Roadmap for Graphene. *Nature* **2012**, *490*, 192–200.
- Castro Neto, A. H.; Guinea, F.; Peres, N. M. R.; Novoselov, K. S.; Geim, A. K. The Electronic Properties of Graphene. *Rev. Mod. Phys.* **2009**, *81*, 109–162.
- Schwierz, F. Graphene Transistors. *Nat. Nanotechnol.* **2010**, *5*, 487–496.
- Georgakilas, V.; Otyepka, M.; Bourlinos, A. B.; Chandra, V.; Kim, N.; Kemp, K. C.; Hobza, P.; Zboril, R.; Kim, K. S. Functionalization of Graphene: Covalent and Noncovalent Approaches, Derivatives and Applications. *Chem. Rev.* **2012**, *112*, 6156–6214.
- Ivanovskii, A. L. Graphene-Based and Graphene-like Materials. *Russ. Chem. Rev.* **2012**, *81*, 571–605.
- Johns, J. E.; Hersam, M. C. Atomic Covalent Functionalization of Graphene. *Acc. Chem. Res.* **2013**, *46*, 77–86.
- Zhang, T.; Xue, Q. Z.; Zhang, S.; Dong, M. D. Theoretical Approaches to Graphene and Graphene-Based Materials. *Nano Today* **2012**, *7*, 180–200.
- Sluiter, M. H. F.; Kawazoe, Y. Cluster Expansion Method for Adsorption: Application to Hydrogen Chemisorption on Graphene. *Phys. Rev. B* **2003**, *68*, 085410.
- Sofo, J. O.; Chaudhari, A. S.; Barber, G. D. Graphane: A Two-Dimensional Hydrocarbon. *Phys. Rev. B* **2007**, *75*, 153401.
- Ryu, S.; Han, M. Y.; Maultzsch, J.; Heinz, T. F.; Kim, P.; Steigerwald, M. L.; Brus, L. E. Reversible Basal Plane Hydrogenation of Graphene. *Nano Lett.* **2008**, *8*, 4597–4602.
- Elias, D. C.; Nair, R. R.; Mohiuddin, T. M. G.; Morozov, S. V.; Blake, P.; Halsall, M. P.; Ferrari, A. C.; Boukhvalov, D. W.; Katsnelson, M. I.; Geim, A. K.; et al. Control of Graphene's Properties by Reversible Hydrogenation: Evidence for Graphane. *Science* **2009**, *323*, 610–613.
- Nair, R. R.; Ren, W. C.; Jalil, R.; Riaz, I.; Kravets, V. G.; Britnell, L.; Blake, P.; Schedin, F.; Mayorov, A. S.; Yuan, S. J.; et al. Fluorographene: A Two-Dimensional Counterpart of Teflon. *Small* **2010**, *6*, 2877–2884.
- Zboril, R.; Karlický, F.; Bourlinos, A. B.; Steriotis, T. A.; Stubos, A. K.; Georgakilas, V.; Safarova, K.; Jancik, D.; Trapalis, C.; Otyepka, M. Graphene Fluoride: A Stable Stoichiometric Graphene Derivative and Its Chemical Conversion to Graphene. *Small* **2010**, *6*, 2885–2891.
- Withers, F.; Dubois, M.; Savchenko, A. K. Electron Properties of Fluorinated Single-Layer Graphene Transistors. *Phys. Rev. B* **2010**, *82*, 073403.
- Rüdorff, W. Graphite Intercalation Compounds. In *Adv. Inorg. Chem. Radiochem.*; Embleton, J., Sharpe, A. G., Eds.; Academic Press: New York, 1959; Vol. 1, pp 223–266.
- Robinson, J. T.; Burgess, J. S.; Junkermeier, C. E.; Badescu, S. C.; Reinecke, T. L.; Perkins, F. K.; Zalalutdinov, M. K.; Baldwin, J. W.; Culbertson, J. C.; Sheehan, P. E.; et al. Properties of Fluorinated Graphene Films. *Nano Lett.* **2010**, *10*, 3001–3005.
- Cheng, S.-H.; Zou, K.; Okino, F.; Gutierrez, H. R.; Gupta, A.; Shen, N.; Eklund, P. C.; Sofo, J. O.; Zhu, J. Reversible Fluorination of Graphene: Evidence of a Two-Dimensional Wide Bandgap Semiconductor. *Phys. Rev. B* **2010**, *81*, 205435.
- Wang, B.; Sparks, J. R.; Gutierrez, H. R.; Okino, F.; Hao, Q. Z.; Tang, Y. J.; Crespi, V. H.; Sofo, J. O.; Zhu, J. Photoluminescence From Nanocrystalline Graphite Monofluoride. *Appl. Phys. Lett.* **2010**, *97*, 141915.
- Chang, H. X.; Cheng, J. S.; Liu, X. Q.; Gao, J. F.; Li, M. J.; Li, J. H.; Tao, X. M.; Ding, F.; Zheng, Z. J. Facile Synthesis of Wide-Bandgap Fluorinated Graphene Semiconductors. *Chem.—Eur. J.* **2011**, *17*, 8896–8903.
- Lee, W. H.; Suk, J. W.; Chou, H.; Lee, J. H.; Hao, Y. F.; Wu, Y. P.; Pineri, R.; Aldrinwande, D.; Kim, K. S.; Ruoff, R. S. Selective-Area Fluorination of Graphene with Fluoropolymer and Laser Irradiation. *Nano Lett.* **2012**, *12*, 2374–2378.
- Wang, Z.; Wang, J.; Li, Z.; Gong, P.; Liu, X.; Zhang, L.; Ren, J.; Wang, H.; Yang, S. Synthesis of Fluorinated Graphene

- with Tunable Degree of Fluorination. *Carbon* **2012**, *50*, 5403–5410.
22. Shen, B. S.; Chen, J. T.; Yan, X. B.; Xue, Q. J. Synthesis of Fluorine-Doped Multi-layered Graphene Sheets by Arc-Discharge. *RSC Adv.* **2012**, *2*, 6761–6764.
 23. Gong, P. W.; Wang, Z. F.; Wang, J. Q.; Wang, H. G.; Li, Z. P.; Fan, Z. J.; Xu, Y.; Han, X. X.; Yang, S. R. One-Pot Sonochemical Preparation of Fluorographene and Selective Tuning of Its Fluorine Coverage. *J. Mater. Chem.* **2012**, *22*, 16950–16956.
 24. Wang, Z.; Wang, J.; Li, Z.; Gong, P.; Ren, J.; Wang, H.; Han, X.; Yang, S. Cooperatively Exfoliated Fluorinated Graphene with Full-Color Emission. *RSC Adv.* **2012**, *2*, 11681–11686.
 25. Li, B.; Zhou, L.; Wu, D.; Peng, H. L.; Yan, K.; Zhou, Y.; Liu, Z. F. Photochemical Chlorination of Graphene. *ACS Nano* **2011**, *5*, 5957–5961.
 26. Wu, J.; Xie, L. M.; Li, Y. G.; Wang, H. L.; Ouyang, Y. J.; Guo, J.; Dai, H. J. Controlled Chlorine Plasma Reaction for Non-invasive Graphene Doping. *J. Am. Chem. Soc.* **2011**, *133*, 19668–19671.
 27. Zheng, J.; Hong-Tao, Liu; Bin, Wu; Chong-An, Di; Yun-Long, Guo; Ti, Wu; Gui, Yu; Liu, Y.-Q.; Zhu, D.-B. Production of Graphite Chloride and Bromide Using Microwave Sparks. *Sci. Rep.* **2012**, *2*, 662.
 28. Gopalakrishnan, K.; Subrahmanyam, K. S.; Kumar, P.; Govindaraj, A.; Rao, C. N. R. Reversible Chemical Storage of Halogens in Few-Layer Graphene. *RSC Adv.* **2012**, *2*, 1605–1608.
 29. Novoselov, K. S.; Geim, A. K.; Morozov, S. V.; Jiang, D.; Zhang, Y.; Dubonos, S. V.; Grigorieva, I. V.; Firsov, A. A. Electric Field Effect in Atomically Thin Carbon Films. *Science* **2004**, *306*, 666–669.
 30. Novoselov, K. S.; Jiang, D.; Schedin, F.; Booth, T. J.; Khotkevich, V. V.; Morozov, S. V.; Geim, A. K. Two-Dimensional Atomic Crystals. *Proc. Natl. Acad. Sci. U.S.A.* **2005**, *102*, 10451–10453.
 31. Jeon, K. J.; Lee, Z.; Pollak, E.; Moreschini, L.; Bostwick, A.; Park, C. M.; Mendelsberg, R.; Radmilovic, V.; Kostecki, R.; Richardson, T. J.; et al. Fluorographene: A Wide Bandgap Semiconductor with Ultraviolet Luminescence. *ACS Nano* **2011**, *5*, 1042–1046.
 32. Bourlinos, A. B.; Safarova, K.; Siskova, K.; Zboril, R. The Production of Chemically Converted Graphenes from Graphite Fluoride. *Carbon* **2012**, *50*, 1425–1428.
 33. Yu, X. X.; Lin, K.; Qiu, K. Q.; Cai, H. B.; Li, X. J.; Liu, J. Y.; Pan, N.; Fu, S. J.; Luo, Y.; Wang, X. P. Increased Chemical Enhancement of Raman Spectra for Molecules Adsorbed on Fluorinated Reduced Graphene Oxide. *Carbon* **2012**, *50*, 4512–4517.
 34. Chen, M. J.; Zhou, H. Q.; Qiu, C. Y.; Yang, H. C.; Yu, F.; Sun, L. F. Layer-Dependent Fluorination and Doping of Graphene via Plasma Treatment. *Nanotechnology* **2012**, *23*, 115706.
 35. Yang, H. C.; Chen, M. J.; Zhou, H. Q.; Qiu, C. Y.; Hu, L. J.; Yu, F.; Chu, W. G.; Sun, S. Q.; Sun, L. F. Preferential and Reversible Fluorination of Monolayer Graphene. *J. Phys. Chem. C* **2011**, *115*, 16844–16848.
 36. Lee, W. K.; Robinson, J. T.; Gunlycke, D.; Stine, R. R.; Tamanaha, C. R.; King, W. P.; Sheehan, P. E. Chemically Isolated Graphene Nanoribbons Reversibly Formed in Fluorographene Using Polymer Nanowire Masks. *Nano Lett.* **2011**, *11*, 5461–5464.
 37. Wheeler, V.; Garces, N.; Nyakiti, L.; Myers-Ward, R.; Jernigan, G.; Culbertson, J.; Eddy, C.; Gaskill, D. K. Fluorine Functionalization of Epitaxial Graphene for Uniform Deposition of Thin High-Kappa Dielectrics. *Carbon* **2012**, *50*, 2307–2314.
 38. Tahara, K.; Iwasaki, T.; Matsutani, A.; Hatano, M. Effect of Radical Fluorination on Mono- and Bi-layer Graphene in Ar/F₂ Plasma. *Appl. Phys. Lett.* **2012**, *101*, 163105.
 39. Sherpa, S. D.; Paniagua, S. A.; Levitin, G.; Marder, S. R.; Williams, M. D.; Hess, D. W. Photoelectron Spectroscopy Studies of Plasma-Fluorinated Epitaxial Graphene. *J. Vac. Sci. Technol. B* **2012**, *30*, 03D102.
 40. Fedorov, V. E.; Grayfer, E. D.; Makotchenko, V. G.; Nazarov, A. S.; Shin, H. J.; Choi, J. Y. Highly Exfoliated Graphite Fluoride as a Precursor for Graphene Fluoride Dispersions and Films. *Croat. Chem. Acta* **2012**, *85*, 107–112.
 41. Withers, F.; Russo, S.; Dubois, M.; Craciun, M. F. Tuning the Electronic Transport Properties of Graphene Through Functionalisation with Fluorine. *Nanoscale Res. Lett.* **2011**, *6*, 526.
 42. Lee, J. H.; Koon, G. K. W.; Shin, D. W.; Fedorov, V. E.; Jae-Young Choi, Yoo, J.-B.; Özilmez, B. Property Control of Graphene by Employing "Semi-Ionic" Liquid Fluorination. *Adv. Funct. Mater.* **2013**, doi: 10.1002/adfm.201202822.
 43. Grayfer, E. D.; Makotchenko, V. G.; Kibis, L. S.; Boronin, A. I.; Pazhetnov, E. M.; Zaikovskii, V. I.; Fedorov, V. E. Synthesis, Properties, and Dispersion of Few-Layer Graphene Fluoride. *Chem. Asian J.* **2013**, doi: 10.1002/asia.201300401.
 44. Pu, L. Y.; Ma, Y. J.; Zhang, W.; Hu, H. L.; Zhou, Y.; Wang, Q. L.; Pei, C. H. Simple Method for the Fluorinated Functionalization of Graphene Oxide. *RSC Adv.* **2013**, *3*, 3881–3884.
 45. Gong, P. W.; Wang, Z. F.; Li, Z. P.; Mi, Y. J.; Sun, J. F.; Niu, L. Y.; Wang, H. G.; Wang, J. Q.; Yang, S. R. Photochemical Synthesis of Fluorinated Graphene via a Simultaneous Fluorination and Reduction Route. *RSC Adv.* **2013**, *3*, 6327–6330.
 46. Kalita, G.; Wakita, K.; Takahashi, M.; Umeno, M. Iodine Doping in Solid Precursor-Based CVD Growth Graphene Film. *J. Mater. Chem.* **2011**, *21*, 15209–15213.
 47. Yao, Z.; Nie, H. G.; Yang, Z.; Zhou, X. M.; Liu, Z.; Huang, S. M. Catalyst-Free Synthesis of Iodine-Doped Graphene via a Facile Thermal Annealing Process and Its Use for Electrocatalytic Oxygen Reduction in an Alkaline Medium. *Chem. Commun.* **2012**, *48*, 1027–1029.
 48. Poh, H. L.; Šimek, P.; Sofer, Z.; Pumera, M. Halogenation of Graphene with Chlorine, Bromine, or Iodine by Exfoliation in a Halogen Atmosphere. *Chem.—Eur. J.* **2013**, *19*, 2655–2662.
 49. Han, S. S.; Yu, T. H.; Merinov, B. V.; van Duin, A. C. T.; Yazami, R.; Goddard, W. A. Unraveling Structural Models of Graphite Fluorides by Density Functional Theory Calculations. *Chem. Mater.* **2010**, *22*, 2142–2154.
 50. Charlier, J. C.; Gonze, X.; Michenaud, J. P. 1st-Principles Study of Graphite Monofluoride (Cf)N. *Phys. Rev. B* **1993**, *47*, 16162–16168.
 51. Touhara, H.; Kadono, K.; Fujii, Y.; Watanabe, N. On the Structure of Graphite Fluoride. *Z. Anorg. Allg. Chem.* **1987**, *544*, 7–20.
 52. Ebert, L. B.; Brauman, J. I.; Huggins, R. A. Carbon Monofluoride—Evidence for a Structure Containing an Infinite Array of Cyclohexane Boats. *J. Am. Chem. Soc.* **1974**, *96*, 7841–7842.
 53. Leenaerts, O.; Peelaers, H.; Hernandez-Nieves, A. D.; Partoens, B.; Peeters, F. M. First-Principles Investigation of Graphene Fluoride and Graphane. *Phys. Rev. B* **2010**, *82*, 195436.
 54. Samarakoon, D. K.; Chen, Z. F.; Nicolas, C.; Wang, X. Q. Structural and Electronic Properties of Fluorographene. *Small* **2011**, *7*, 965–969.
 55. Samarakoon, D. K.; Wang, X. Q. Chair and Twist-Boat Membranes in Hydrogenated Graphene. *ACS Nano* **2009**, *3*, 4017–4022.
 56. Klintenberg, M.; Lebegue, S.; Katsnelson, M. I.; Eriksson, O. Theoretical Analysis of the Chemical Bonding and Electronic Structure of Graphene Interacting with Group IA and Group VIIA Elements. *Phys. Rev. B* **2010**, *81*, 085433.
 57. Medeiros, P. V. C.; Mascarenhas, A. J. S.; Mota, F. D.; de Castilho, C. M. C. A DFT Study of Halogen Atoms Adsorbed on Graphene Layers. *Nanotechnology* **2010**, *21*, 485701.
 58. Karlicky, F.; Zboril, R.; Otyepka, M. Band Gaps and Structural Properties of Graphene Halides and Their Derivatives: A Hybrid Functional Study with Localized Orbital Basis Sets. *J. Chem. Phys.* **2012**, *137*, 034709.

59. Karlicky, F.; Otyepka, M. Band Gap and Optical Spectra of Chlorographene, Fluorographene and Graphane from G0W0, GW0 and GW Calculations on Top of PBE and HSE06 Orbitals. *J. Chem. Theory Comput.* **2013**, DOI: 10.1021/ct400476r.
60. Kwon, S.; Ko, J. H.; Jeon, K. J.; Kim, Y. H.; Park, J. Y. Enhanced Nanoscale Friction on Fluorinated Graphene. *Nano Lett.* **2012**, *12*, 6043–6048.
61. Zhou, J.; Liang, Q. F.; Dong, J. M. Enhanced Spin-Orbit Coupling in Hydrogenated and Fluorinated Graphene. *Carbon* **2010**, *48*, 1405–1409.
62. Munoz, E.; Singh, A. K.; Ribas, M. A.; Penev, E. S.; Yakobson, B. I. The Ultimate Diamond Slab: Graphene versus Graphene. *Diam. Relat. Mater.* **2010**, *19*, 368–373.
63. Ribas, M. A.; Singh, A. K.; Sorokin, P. B.; Yakobson, B. I. Patterning Nanoroads and Quantum Dots on Fluorinated Graphene. *Nano Res.* **2011**, *4*, 143–152.
64. Takagi, Y.; Kusakabe, K. Transition from Direct Band Gap to Indirect Band Gap in Fluorinated Carbon. *Phys. Rev. B* **2002**, *65*, 121103(R).
65. Heyd, J.; Scuseria, G. E.; Ernzerhof, M. Hybrid Functionals Based on a Screened Coulomb Potential. *J. Chem. Phys.* **2003**, *118*, 8207–8215.
66. Barone, V.; Hod, O.; Peralta, J. E.; Scuseria, G. E. Accurate Prediction of the Electronic Properties of Low-Dimensional Graphene Derivatives Using a Screened Hybrid Density Functional. *Acc. Chem. Res.* **2011**, *44*, 269–279.
67. Krkau, A. V.; Vydrov, O. A.; Izmaylov, A. F.; Scuseria, G. E. Influence of the Exchange Screening Parameter on the Performance of Screened Hybrid Functionals. *J. Chem. Phys.* **2006**, *125*, 224106.
68. Liang, Y.; Yang, L. Electronic Structure and Optical Absorption of Fluorographene. *MRS Proc.* **2011**, *1370*, 137.
69. Sahin, H.; Topsakal, M.; Ciraci, S. Structures of Fluorinated Graphene and Their Signatures. *Phys. Rev. B* **2011**, *83*, 115432.
70. Wei, W.; Jacob, T. Electronic and Optical Properties of Fluorinated Graphene: A Many-Body Perturbation Theory Study. *Phys. Rev. B* **2013**, *87*, 115431.
71. Peelaers, H.; Hernandez-Nieves, A. D.; Leenaerts, O.; Partoens, B.; Peeters, F. M. Vibrational Properties of Graphene Fluoride and Graphane. *Appl. Phys. Lett.* **2011**, *98*, 051914.
72. Bon, S. B.; Valentini, L.; Verdejo, R.; Fierro, J. L. G.; Peponi, L.; Lopez-Manchado, M. A.; Kenny, J. M. Plasma Fluorination of Chemically Derived Graphene Sheets and Subsequent Modification with Butylamine. *Chem. Mater.* **2009**, *21*, 3433–3438.
73. Wang, Y.; Lee, W. C.; Manga, K. K.; Ang, P. K.; Lu, J.; Liu, Y. P.; Lim, C. T.; Loh, K. P. Fluorinated Graphene for Promoting Neuro-induction of Stem Cells. *Adv. Mater.* **2012**, *24*, 4285–4290.
74. Singh, S. K.; Srinivasan, S. G.; Neek-Amal, M.; Costamagna, S.; van Duin, A. C. T.; Peeters, F. M. Thermal Properties of Fluorinated Graphene. *Phys. Rev. B* **2013**, *87*, 104114.
75. Sahin, H.; Ciraci, S. Chlorine Adsorption on Graphene: Chlorographene. *J. Phys. Chem. C* **2012**, *116*, 24075–24083.
76. Ko, J. H.; Kwon, S.; Byun, I. S.; Choi, J. S.; Park, B. H.; Kim, Y. H.; Park, J. Y. Nanotribological Properties of Fluorinated, Hydrogenated, and Oxidized Graphenes. *Tribol. Lett.* **2013**, *50*, 137–144.
77. Wang, L.-F.; Ma, T.-B.; Hu, Y.-Z.; Wang, H.; Shao, T.-M. *Ab-Initio* Study on the Friction Mechanism of Fluorographene and Graphane. *J. Phys. Chem. C* **2013**, *117*, 12520–12525.
78. Bourlinos, A. B.; Bakandritsos, A.; Liaros, N.; Couris, S.; Safarova, K.; Otyepka, M.; Zboril, R. Water Dispersible Functionalized Graphene Fluoride with Significant Non-linear Optical Response. *Chem. Phys. Lett.* **2012**, *543*, 101–105.
79. Kita, Y.; Watanabe, N.; Fujii, Y. Chemical Composition and Crystal-Structure of Graphite Fluoride. *J. Am. Chem. Soc.* **1979**, *101*, 3832–3841.
80. Markevich, A.; Jones, R.; Briddon, P. R. Doping of Fluorographene by Surface Adsorbates. *Phys. Rev. B* **2011**, *84*, 115439.
81. Nava, M.; Galli, D. E.; Cole, M. W.; Reatto, L. Adsorption of He Isotopes on Fluorographene and Graphane: Fluid and Superfluid Phases from Quantum Monte Carlo Calculations. *Phys. Rev. B* **2012**, *86*, 174509.
82. Osuna, S.; Torrent-Sucarrat, M.; Sola, M.; Geerlings, P.; Ewels, C. P.; Van Lier, G. Reaction Mechanisms for Graphene and Carbon Nanotube Fluorination. *J. Phys. Chem. C* **2010**, *114*, 3340–3345.
83. Liu, H. Y.; Hou, Z. F.; Hu, C. H.; Yang, Y.; Zhu, Z. Z. Electronic and Magnetic Properties of Fluorinated Graphene with Different Coverage of Fluorine. *J. Phys. Chem. C* **2012**, *116*, 18193–18201.
84. Neek-Amal, M.; Beheshtian, J.; Shayeganfar, F.; Singh, S. K.; Los, J. H.; Peeters, F. M. Spiral Graphene and One-Sided Fluorographene Nanoribbons. *Phys. Rev. B* **2013**, *87*, 075448.
85. Chantharasupawong, P.; Philip, R.; Narayanan, N. T.; Sudeep, P. M.; Mathkar, A.; Ajayan, P. M.; Thomas, J. Optical Power Limiting in Fluorinated Graphene Oxide: An Insight into the Nonlinear Optical Properties. *J. Phys. Chem. C* **2012**, *116*, 25955–25961.
86. Hong, X.; Cheng, S. H.; Herding, C.; Zhu, J. Colossal Negative Magnetoresistance in Dilute Fluorinated Graphene. *Phys. Rev. B* **2011**, *83*, 085410.
87. Hong, X.; Zou, K.; Wang, B.; Cheng, S. H.; Zhu, J. Evidence for Spin-Flip Scattering and Local Moments in Dilute Fluorinated Graphene. *Phys. Rev. Lett.* **2012**, *108*, 226602.
88. Sofo, J. O.; Suarez, A. M.; Usaj, G.; Cornaglia, P. S.; Hernandez-Nieves, A. D.; Balseiro, C. A. Electrical Control of the Chemical Bonding of Fluorine on Graphene. *Phys. Rev. B* **2011**, *83*, 081411.
89. Nair, R. R.; Seponi, M.; Tsai, I. L.; Lehtinen, O.; Keinonen, J.; Krasheninnikov, A. V.; Thomson, T.; Geim, A. K.; Grigorieva, I. V. Spin-Half Paramagnetism in Graphene Induced by Point Defects. *Nat. Phys.* **2012**, *8*, 199–202.
90. Okotrub, A. V.; Yudanov, N. F.; Asanov, I. P.; Vyalikh, D. V.; Bulusheva, L. G. Anisotropy of Chemical Bonding in Semifluorinated Graphite C₂F Revealed with Angle-Resolved X-ray Absorption Spectroscopy. *ACS Nano* **2012**, *7*, 65–74.
91. Huang, W. X.; Pei, Q. X.; Liu, Z. S.; Zhang, Y. W. Thermal Conductivity of Fluorinated Graphene: A Non-equilibrium Molecular Dynamics Study. *Chem. Phys. Lett.* **2012**, *552*, 97–101.
92. Schrier, J. Fluorinated and Nanoporous Graphene Materials as Sorbents for Gas Separations. *ACS Appl. Mater. Interfaces* **2011**, *3*, 4451–4458.
93. Raghavan, S.; Denig, T. J.; Nelson, T. C.; Stinespring, C. D. Novel Surface Chemical Synthesis Route for Large Area Graphene-on-Insulator Films. *J. Vac. Sci. Technol. B* **2012**, *30*, 030605.
94. Cheng, H. S.; Sha, X. W.; Chen, L.; Cooper, A. C.; Foo, M. L.; Lau, G. C.; Bailey, W. H.; Pez, G. P. An Enhanced Hydrogen Adsorption Enthalpy for Fluoride Intercalated Graphite Compounds. *J. Am. Chem. Soc.* **2009**, *131*, 17732–17733.
95. Mathkar, A.; Narayanan, T. N.; Alemany, L. B.; Cox, P.; Nguyen, P.; Gao, G. H.; Chang, P.; Romero-Aburto, R.; Mani, S. A.; Ajayan, P. M. Synthesis of Fluorinated Graphene Oxide and its Amphiphobic Properties. *Part. Part. Syst. Char.* **2013**, *30*, 266–272.
96. Sivek, J.; Leenaerts, O.; Partoens, B.; Peeters, F. M. First-Principles Investigation of Bilayer Fluorographene. *J. Phys. Chem. C* **2012**, *116*, 19240–19245.
97. Hu, C. H.; Zhang, P.; Liu, H. Y.; Wu, S. Q.; Yang, Y.; Zhu, Z. Z. Structural Stability and Electronic and Magnetic Properties of Fluorinated Bilayer Graphene. *J. Phys. Chem. C* **2013**, *117*, 3572–3579.
98. Ueta, A.; Tanimura, Y.; Prezhdo, O. V. Infrared Spectral Signatures of Multilayered Surface-Fluorinated Graphene: A Molecular Dynamics Study. *J. Phys. Chem. C* **2012**, *116*, 8343–8347.

99. Ueta, A.; Tanimura, Y.; Prezhdo, O. V. Infrared Spectral Signatures of Surface-Fluorinated Graphene: A Molecular Dynamics Study. *J. Phys. Chem. Lett.* **2012**, *3*, 246–250.
100. Li, Y. F.; Li, F. Y.; Chen, Z. F. Graphane/Fluorographene Bilayer: Considerable C-H...F-C Hydrogen Bonding and Effective Band Structure Engineering. *J. Am. Chem. Soc.* **2012**, *134*, 11269–11275.
101. Yang, M. M.; Zhou, L.; Wang, J. Y.; Liu, Z. F.; Liu, Z. R. Evolutionary Chlorination of Graphene: From Charge-Transfer Complex to Covalent Bonding and Nonbonding. *J. Phys. Chem. C* **2012**, *116*, 844–850.
102. Ijas, M.; Havu, P.; Harju, A. Fracturing Graphene by Chlorination: A Theoretical Viewpoint. *Phys. Rev. B* **2012**, *85*, 035440.
103. Kim, J. Y.; Lee, W. H.; Suk, J. W.; Potts, J. R.; Chou, H.; Kholmanov, I. N.; Piner, R. D.; Lee, J.; Akinwande, D.; Ruoff, R. S. Chlorination of Reduced Graphene Oxide Enhances the Dielectric Constant of Reduced Graphene Oxide/Polymer Composites. *Adv. Mater.* **2013**, *25*, 2308–2313.
104. Jung, N.; Kim, N.; Jockusch, S.; Turro, N. J.; Kim, P.; Brus, L. Charge Transfer Chemical Doping of Few Layer Graphenes: Charge Distribution and Band Gap Formation. *Nano Lett.* **2009**, *9*, 4133–4137.
105. Yaya, A.; Ewels, C. P.; Suarez-Martinez, I.; Wagner, P.; Lefrant, S.; Okotrub, A.; Bulusheva, L.; Briddon, P. R. Bromination of Graphene and Graphite. *Phys. Rev. B* **2011**, *83*, 045411.
106. Ghosh, S.; Yamijala, S. R. K. C. S.; Pati, S. K.; Rao, C. N. R. The Interaction of Halogen Molecules with SWNTs and Graphene. *RSC Adv.* **2012**, *2*, 1181–1188.
107. Boukhvalov, D. W.; Katsnelson, M. I. Chemical Functionalization of Graphene. *J. Phys. Condens. Mater.* **2009**, *21*, 344205.
108. Ong, M. T.; Duerloo, K.-A. N.; Reed, E. J. The Effect of Hydrogen and Fluorine Coadsorption on the Piezoelectric Properties of Graphene. *J. Phys. Chem. C* **2013**, *117*, 3615–3620.
109. Shi, H. L.; Pan, H.; Zhang, Y. W.; Yakobson, B. I. Electronic and Magnetic Properties of Graphene/Fluorographene Superlattices. *J. Phys. Chem. C* **2012**, *116*, 18278–18283.
110. Xie, H.; Lu, W.-C.; Zhang, W.; Qin, P.-H.; Wang, C. Z.; Ho, K. M. Electronic and Magnetic Properties of Triangular Graphene Nanoflakes Embedded in Fluorographene. *Chem. Phys. Lett.* **2013**, *572*, 48–52.
111. Singh, A. K.; Yakobson, B. I. Electronics and Magnetism of Patterned Graphene Nanoroads. *Nano Lett.* **2009**, *9*, 1540–1543.
112. Hernandez-Nieves, A. D.; Partoens, B.; Peeters, F. M. Electronic and Magnetic Properties of Superlattices of Graphene/Graphane Nanoribbons with Different Edge Hydrogenation. *Phys. Rev. B* **2010**, *82*, 165412.
113. Ao, Z. M.; Hernandez-Nieves, A. D.; Peeters, F. M.; Li, S. Enhanced Stability of Hydrogen Atoms at the Graphene/Graphane Interface of Nanoribbons. *Appl. Phys. Lett.* **2010**, *97*, 233109.
114. Singh, A. K.; Penev, E. S.; Yakobson, B. I. Vacancy Clusters in Graphane as Quantum Dots. *ACS Nano* **2010**, *4*, 3510–3514.
115. Tang, S. B.; Zhang, S. Y. Structural and Electronic Properties of Hybrid Fluorographene—Graphene Nanoribbons: Insight from First-Principles Calculations. *J. Phys. Chem. C* **2011**, *115*, 16644–16651.
116. Withers, F.; Bointon, T. H.; Dubois, M.; Russo, S.; Craciun, M. F. Nanopatterning of Fluorinated Graphene by Electron Beam Irradiation. *Nano Lett.* **2011**, *11*, 3912–3916.
117. Feng, Q.; Cao, Q.; Li, M.; Liu, F.; Tang, N.; Du, Y. Synthesis and Photoluminescence of Fluorinated Graphene Quantum Dots. *Appl. Phys. Lett.* **2013**, *102*, 013111.
118. Zhang, L. M.; Yu, J. W.; Yang, M. M.; Xie, Q.; Peng, H. L.; Liu, Z. F. Janus Graphene from Asymmetric Two-Dimensional Chemistry. *Nat. Commun.* **2013**, *4*, 1443.